

1 **The physical properties of coarse fragment soils and their**
2 **effects on permafrost dynamics: A case study on the**
3 **central Qinghai-Tibetan Plateau**

4 **Shuhua Yi^{1,2}, Yujie He^{3*}, Xinlei Guo⁴, Jianjun Chen^{5,6}, Qingbai Wu⁷, Yu Qin²,**
5 **and Yongjian Ding^{2,8,9}**

6 ^{1.} School of Geographic Sciences, Nantong University, 999 Tongjing Road, Nantong, 226007,
7 China

8 ^{2.} State Key Laboratory of Cryospheric Sciences, Northwest Institute of Eco-Environment and
9 Resources, Chinese Academy of Sciences, 320 Donggang West Road, 730000, Lanzhou,
10 Gansu, China

11 ^{3.} Chinese Research Academy of Environmental Sciences, No.8 Dayangfang, Chaoyang
12 District, 100012, Beijing, China

13 ^{4.} Department of Ecosystem and Landscape Dynamics, Institute for Biodiversity and
14 Ecosystem Dynamics, University of Amsterdam, Science Park 904, 1098 XH Amsterdam,
15 The Netherlands

16 ^{5.} College of Geomatics and Geoinformation, Guilin University of Technology, 12 Jiangan
17 Road, Guilin, 541004, China

18 ^{6.} Guangxi Key Laboratory of Spatial Information and Geomatics, 12 Jiangan Road, Guilin,
19 541004, China

20 ^{7.} State Key Laboratory of Frozen Soil Engineering, Northwest Institute of Eco-Environment
21 and Resources, Chinese Academy of Sciences, 320 Donggang West Road, 730000,
22 Lanzhou, Gansu, China

23 ^{8.} Key Laboratory of Ecohydrology of Inland River Basin, Chinese Academy of Sciences,
24 Lanzhou 730000, China

25 ^{9.} University of Chinese Academy Sciences, Beijing, 100049, China

26 *Co-first Author

27 *Correspondence to:* Yongjian Ding (dyj@lzb.ac.cn)

28 **Abstract.** Soils on the Qinghai-Tibetan Plateau (QTP) have distinct physical properties from
29 agricultural soils due to weak weathering and strong erosion. These properties might affect
30 permafrost dynamics. However, few studies have investigated both quantitatively. In this
31 study, we selected a permafrost site on the central region of the QTP and excavated soil
32 samples down, to 200 cm. We measured soil porosity, thermal conductivity, saturated
33 hydraulic conductivity and matric potential in the laboratory. Finally, we ran a simulation
34 model replacing default sand or loam parameters with different combinations of these
35 measured parameters. Our results from the soil profile showed that coarse fragment soil
36 (diameter >2 mm) was ~55% on average in soil profile, soil porosity was less than $0.3 \text{ m}^3 \text{ m}^{-3}$,

1 saturated hydraulic conductivity ranged from 0.004-0.03 mm s⁻¹, saturated matric potential
2 ranged from -14 to -604 mm. When default sand or loam parameters were substituted with
3 these measured values, the model errors of soil temperature, soil liquid water content, active
4 layer depth and permafrost lower boundary were reduced. The root mean squared errors of
5 active layer depths simulated using measured parameters versus the default sand and loam
6 parameters were about 0.28, 1.06, 1.83 m, respectively. Among these measured parameters,
7 porosities, which were much smaller than for soil textures used in land surface models, played
8 a dominant role in reducing model errors. We also demonstrated that soil water dynamic
9 processes should be considered, rather than using static properties under frozen and unfrozen
10 soil states as in most permafrost models. We conclude that it is necessary to consider the
11 distinct physical properties of soil and water dynamics on the QTP when simulating dynamics
12 of permafrost. It is important to develop methods for systematic measuring physical
13 properties of coarse fragment soils and to develop a spatial dataset for porosity because of its
14 importance in simulating permafrost dynamics in this region.

15 **Key words:** Terrestrial Ecosystem Model; Active layer; Sensitivity test; Soil temperature;
16 Soil water content; Porosity; Coarse fragment soils

17 **1 Introduction**

18 Permafrost covers 25% of Earth's surface. Degradation of permafrost has been reported
19 extensively in Alaska, Siberia and the Qinghai-Tibetan Plateau (QTP; Boike et al., 2013;
20 Jorgenson et al., 2006; Wu and Zhang, 2010). Permafrost thaw has global impacts by
21 releasing large quantities of soil carbon previously preserved in a frozen state and enhancing
22 concentrations of atmospheric greenhouse gases, which will promote further atmospheric
23 warming and degradation of permafrost (Anisimov, 2007; McGuire et al., 2009). Permafrost
24 dynamics also have local to regional impacts on ecosystems by altering soil thermal and
25 hydrological regimes (Salmon et al., 2015; Wang et al., 2008; Wright et al., 2009; Ye et al.,
26 2009; Yi et al., 2014a). In addition, degradation of permafrost affects infrastructure, such as
27 QTP railways and roads (Wu et al., 2004) or the Trans-Alaska Pipeline System in Alaska
28 (Nelson et al., 2001). Therefore, it is critical to develop mitigation and adaptation strategies in
29 permafrost regions for ongoing climate change. Accurate projection of the degree of
30 permafrost degradation is a prerequisite for developing these strategies.

31 Significant effort has been made to improve modeling accuracy and efficiency of

1 permafrost dynamics along two primary lines of inquiry. One is to create suitable freezing and
2 thawing algorithms for different applications, including land surface models (Chen et al.,
3 2015; Oleson et al., 2010; Wang et al., 2017), permafrost models (Goodrich, 1978; Langer et
4 al., 2013; Qin et al., 2017), and other related models (Fox, 1992; Woo et al., 2004). The other
5 line of inquiry is focused on schemes of soil physical properties (Chen et al., 2012; Zhang et
6 al., 2011), which play a critical role in permafrost dynamics. For example, porosity
7 determines the maximum amount of water that can be contained in a soil layer, thermal
8 properties determine the heat conduction within soil layers, and hydraulic properties
9 determine the exchange of soil water between soil layers. The soil water content also
10 determines the large amount of latent heat lost or gained by freezing or thawing, respectively.
11 On the QTP, soil is coarse due to weak weathering and strong erosion (Arocena et al., 2012).
12 Soils with gravel content (particle diameter >2 mm) have been reported in several studies
13 (Wang et al., 2011; Wu et al., 2016; Yang et al., 2009; Qin et al., 2015; Chen et al., 2017; Du
14 et al., 2017). These gravelly soil properties are likely different from those used in current
15 modeling studies (Wang et al., 2013). For example, soil properties in Community Land Model
16 are calculated from fractions of sand, silt and clay based on measurements of agriculture soils
17 (Oleson et al., 2010). However, soil properties of coarse fragment soil on the QTP and their
18 effects on permafrost dynamics are under studied (Pan et al., 2017).

19 In this case study we investigated the characteristics of soil physical properties at a site on
20 the central QTP and their effects on permafrost dynamics. We first measured soil physical
21 properties of excavated soil samples in a laboratory. We then conducted sensitivity analysis
22 with an ecosystem model by substituting the default soil physical properties with those that
23 we measured. We aimed to emphasize the effects of coarse fragment content on soil physical
24 properties and on permafrost dynamics, rather than develop general schemes of soil physical
25 properties for using in modeling studies on the QTP.

26 **2 Methods**

27 **2.1 Site description**

28 The site (34°49'46.2" N, 92°55'56.58" E, 4,628ma.s.l.) is located in the Beiluhe basin, in the
29 continuous permafrost region of the central QTP (Figure 1a, Zou et al. 2017). Based on the
30 map of Li et al. (2015), soils of this region belong to Gelisols and Inceptisols, which occupy
31 34% and 28% of the total area of permafrost region of the QTP, respectively. Land surface
32 types include alpine meadow, alpine steppe, barren surface and thermokarst lakes (Figure 1b;

1 Lin et al., 2011).

2 The site is on top of upland plain landforms, which are formed from fluvial and deluvial
3 sediments. The surficial sediments are dominated by fine to gravelly sands and stones (Figure
4 2; Yin et al., 2017). Soil of this site belongs to Inceptisols (Dr. Li, Wangping of Lanzhou
5 University of Technology, personal communication). Mudstone is common beneath soil. The
6 plant community type is mainly alpine meadow which is dominated by monocotyledonous
7 species, primarily Poaceae and Cyperaceae. The dominant species are *Kobresia pygmaea*,
8 accompanied *Elymus nutans*, *Carex moorcroftii*, *Oxytropis pusilla*, *Tibetia himalaica*,
9 *Leontopodium nanum* and *Androsace tapete* (Figure 2c-e).

10 A weather station was set up in 2002 (Figure 2a) to measure air temperature and relative
11 humidity (2.2m, HMP45C-L11 /L36, Campbell Scientific Inc.), solar radiation (MS-102,
12 EKO, Japan) and precipitation (QMR102, Vaisala Company). Soil temperatures were
13 measured at depths of 5, 10, 20, 40, 80 and 160 cm using a PT-100 (EKO, Japan); soil
14 moistures were measured at depths of 20, 40, 80 and 160 cm using a CS616-L50 (EKO,
15 Japan). A CR3000 data logger (Campbell Scientific Inc., USA) was used to store these data at
16 30 minute intervals. These readings were averaged or summed (e.g. precipitation) into
17 monthly values to drive and validate the model. Based on measurements, multi-year mean
18 annual air temperature, precipitation, downward solar radiation and relative humidity were -
19 3.61 °C, 365.7 mm, 206.3 W m⁻² and 51.1%, respectively (Figure 3). The multi-year mean
20 summer (June to August) air temperature and precipitation were 5.27 °C and 248.3 mm,
21 respectively. The multi-year mean winter (December to February) air temperature and
22 precipitation were -12.44 °C and 5.3 mm, respectively. The multi-year mean annual, summer,
23 winter soil temperature at 40 cm were 0.17, 6.65 and -7.15 °C, respectively. Those at 80 cm
24 were 0.11, 4.32 and -4.86 °C, respectively

25 A borehole was drilled in 2002, and thermistors made by the State Key Laboratory of
26 Frozen Soil Engineering, Chinese Academy of Sciences were installed at 0.5 m intervals from
27 0.5 to 10 m, at 2 m intervals from 12 to 30 m, at 4 m intervals from 34 to 50 m,, and at 55 and
28 60 m. Temperature accuracy of this type of thermistor is ±0.05 °C (Wu et al., 2016). The
29 temperatures were recorded on the 5th and 20th days of each month using CR3000 data
30 logger (Campbell Scientific Inc., USA). Based on measurement, active layer depth is ~3.3 m,
31 depth of zero annual amplitude is ~6.2 m, and the lower boundary of permafrost is at a depth
32 of ~20 m. The multi-year mean ground temperatures at 0.5, 6, and 60 m are about -0.52, -0.30
33 and 1.81 °C, respectively.

1

2 **2.2 Soil sampling and measurement**

3 Permafrost dynamics are affected by atmosphere, vegetation, and soil textures, therefore, we
4 excavated soil close to the weather station and borehole (Figure 2a) down to 2 m (Figure 2b) in
5 August 2014. We used cut rings (10 cm diameter, 6.37 cm height and 500 cm³) to take soil
6 samples at depth ranges of 0-10, 10-20, 20-30, 40-50, 70-80, 110-120, 150-160, and 190-200
7 cm. Three replicates were sampled from the top of each depth range and sealed for analysis in
8 the laboratory. Above 120 cm in the soil pit, coarse soil material was small enough in the cut
9 rings. Below 150 cm, the material is weathered mudstone, which could also be sampled with
10 our cut rings. Based on the excavated soil pit and measured soil temperature, this site belongs to
11 Inceptisols with suborder of Gelept (soil taxonomy, ST, Soil Survey Staff, 2014). The soil pit
12 consists of A horizon (~20 cm), Bw horizon (~20-80 cm) and C material dominated by
13 fractured bedrock.

14 We used the KD2 Pro (Decagon, US) to measure thermal conductivity of soil samples. The
15 steps we took to determine soil properties for each sample were as follows: 1) soil sample was
16 dried in an oven and weighed (0.001g precision) to calculate bulk density; Then 2) the soil
17 sample was exposed to a constant temperature (20°C) for 24 h, a certain volume of water was
18 injected into the soil samples, and KD2 Pro (Decagon, USA) was used to measure the thermal
19 conductivity, Next 3) the sample and the KD2 probe were put into a refrigerator at -15°C for 12
20 h and thermal conductivity was measured again; 4) Steps 2 and 3 were repeated at increasing
21 levels of soil volumetric water content until soil samples were up to the point of saturation.
22 Finally 5), the soil sample was immersed in water for 24 h and weighed to calculate porosity,
23 and the saturated unfrozen and frozen thermal conductivity were then measured, accordingly.
24 The bulk density (BD), porosity (PORO) and volumetric water content (VWC) were calculated
25 with the following equations.

$$26 \quad BD = \frac{W_{dry} - W_{cr}}{V_{cr}} \quad (1)$$

$$27 \quad PORO = \frac{W_{sat} - W_{dry}}{V_{cr}} / \rho \quad (2)$$

$$28 \quad VWC = \frac{W_{all} - W_{dry}}{V_{cr}} / \rho \quad (3)$$

1 Where W_{dry} , W_{sat} , W_{all} , W_{cr} are mass of over dried sample, saturated sample, sample with
2 some water with cut ring, and empty cut ring (g), respectively. V_{cr} is the volume of cut ring
3 (cm^3). ρ is the density of water (1 g cm^{-3}). We used pressure membrane instruments (1500F1,
4 Soilmoisture Equipment Corp, US) to measure the matric potential of soil samples (Azam et al.,
5 2014; Wang et al., 2007), using both 15 bar and 5 bar pressure chambers. Pressure values were
6 set at 0, 10, 20, 40, 60, 80, 100, 150, 200, 300, and 400 kpa. It usually took 3-4 days to finish
7 one measurement at one pressure level. We used a soil permeability meter (TST-70, Nanjing T-
8 Bota Sciotech Instruments & Equipment Co., Ltd. China) to measure saturated hydraulic
9 conductivity of soil samples (Gwenzi et al., 2011). Finally, soil samples were sieved through a
10 2.0 mm mesh, and soil particle size distribution was determined with a laser diffraction
11 analyzer (Malvern-2000, Worcestershire, UK).

12 **2.3 Model description**

13 The model used in this study is a dynamic organic soil version of Terrestrial Ecosystem
14 Model (DOS-TEM). Models from the TEM family simulate the carbon and nitrogen pools of
15 vegetation and soil, and their fluxes among atmosphere, vegetation, and soil (McGuire et al.,
16 1992). They have been widely used in studies of cold region ecosystems (e.g. McGuire et al.,
17 2000; Yuan et al., 2012; Zhuang et al., 2004; 2010). The DOS-TEM consists of four modules,
18 environmental, ecological, fire disturbance, and dynamic organic soil (Yi et al., 2010). The
19 environmental module operates on a daily time interval using mean daily air temperature,
20 surface solar radiation, precipitation, and vapor pressure, which are downscaled from monthly
21 input data (Yi et al., 2009b). The module takes into account radiation and water fluxes among
22 the atmosphere, canopy, snow pack, and soil. Soil temperatures, soil liquid water content,
23 temperature in rock layers, active layer depth (ALD) and permafrost low boundary (PLB)
24 were simulated explicitly.

25 **2.3.1 Implementation of soil thermal processes**

26 Earlier versions of TEM did not simulate soil temperature (McGuire et al., 1992). Zhuang et
27 al. (2001) incorporated Goodrich (1978) permafrost model into TEM. Yi et al. (2009a)
28 incorporated a two-directional Stefan algorithm to simulate soil freezing and thawing for
29 complex soils with changes in soil organic and moisture content. Temperatures of all soil
30 layers in the DOS-TEM are updated daily. Phase change is calculated first before heat

1 conduction. A two-directional Stefan algorithm is used to predict the depths of freezing or
 2 thawing fronts within the soil (Woo et al., 2004). It first simulates the depth of the front in the
 3 soil column from the top downward, using soil surface temperature as the driving temperature.
 4 It then simulates the front from the bottom upward using the soil temperature at a specified
 5 depth beneath a front as the driving temperature (bottom-up forcing). The latent heat used for
 6 phase change is recorded for each soil layer. If a layer contains n freezing or thawing fronts,
 7 this layer is then explicitly divided into $n+1$ soil layers. All soil layers are grouped into 3 parts:
 8 1) those above the uppermost freezing or thawing front; 2) those below the lowermost
 9 freezing or thawing front; and 3) those between the uppermost and lowermost fronts. Soil
 10 temperatures are then updated by solving finite difference equations of each part with latent
 11 heat from phase change as an energy source or sink (Yi et al., 2014a). Soil surface
 12 temperature, which is used as a boundary condition, is calculated using daily air maximum,
 13 air minimum, radiation, and leaf area index (Yi et al., 2013).

14 The version of the DOS-TEM in this study uses the Côté and Konrad (2005) scheme to
 15 calculate thermal conductivity (Yi et al., 2013; Pan et al., 2017), which is also been used by
 16 other studies on the QTP (e.g. Chen et al., 2012, Luo et al., 2009), and is as follows:

$$17 \quad \lambda = \begin{cases} k_e \lambda_{sat} + (1 - k_e) \lambda_{dry} & s > 10^{-5} \\ \lambda_{dry} & s \leq 10^{-5} \end{cases} \quad (4)$$

18 where λ , λ_{sat} , λ_{dry} are soil thermal conductivity, saturated soil thermal conductivity, and dry
 19 soil thermal conductivity ($\text{W m}^{-1} \text{K}^{-1}$), respectively, and k_e is the Kersten number (Côté and
 20 Konrad, 2005). Dry thermal conductivity varies with soil properties according to:

$$21 \quad \lambda_{dry} = \chi 10^{-\eta \phi} \quad (5)$$

22 where χ ($\text{W m}^{-1} \text{K}^{-1}$) and η (no unit) are parameters accounting for particle shape effects,
 23 which are specified for gravel, fine mineral and organic soil (Côté and Konrad, 2005), and ϕ
 24 is porosity. Saturated thermal conductivity varies with water content and phase state
 25 according to:

$$26 \quad \lambda_{sat} = \begin{cases} \lambda_s^{1-\phi} \lambda_{liq}^\phi & T \leq T_f \\ \lambda_s^{1-\phi} \lambda_{ice}^\phi & T > T_f \end{cases} \quad (6)$$

27 where λ_{liq} , λ_{ice} , λ_s are thermal conductivities of liquid water, ice, and soil solid ($\text{W m}^{-1} \text{K}^{-1}$),
 28 which are all constant values. T and T_f are temperature of soil and freezing point temperature

1 of soil (°C), respectively. In DOS-TEM, freezing or thawing processes are assumed to be
2 happened at T_f , following most of the land surface models (e.g. Oleson et al. 2010).

3 **2.3.2 Implementation of soil hydrological processes**

4 Surface runoff, infiltration, and water redistribution among soil layers are simulated in a
5 similar way as Community Land Model 4 (Oleson et al., 2010). Soil matric potential (Ψ)
6 determines the direction of water movement, and hydraulic conductivity describes the ease
7 with which water can move through the soil.

$$8 \quad \Psi = \Psi_{sat} \left(\frac{\theta_{liq}}{\phi} \right)^{-B} \quad (7)$$

9 where Ψ_{sat} is saturated soil matric potential (mm H₂O, hereafter mm), θ_{liq} is volumetric
10 liquid water content (m³ m⁻³), and B is pore size distribution parameter. The soil hydraulic
11 conductivity (K, mm s⁻¹) is a function of the saturated soil hydraulic conductivity (K_{sat}) as
12 follows:

$$13 \quad K = K_{sat} \left(\frac{\theta_{liq}}{\phi} \right)^{2B+3} \quad (8)$$

14 Several important features relating to permafrost have been considered in the DOS-TEM
15 (see Yi et al., 2014b), including runoff from a perched saturated zone or exchanges of water
16 between the soil and a water reservoir. Runoff from a perched saturated zone above
17 permafrost is implemented following Swenson et al. (2013):

$$18 \quad Q_{perch} = \alpha k_p (z_{frost} - z_{perched}) \sin\left(\frac{\Theta}{180} \pi\right) \quad (9)$$

19 where α is an adjustable parameter (0.6 m⁻¹), K_p is the mean saturated hydraulic conductivity
20 within the perched saturated zone (mm s⁻¹), z_{frost} and $z_{perched}$ are the depths to the permafrost
21 table and the perched water table (m), respectively, and Θ is slope (°).

22 The DOS-TEM has been verified against the Neumann Equation for water, mineral and
23 organic soil under an idealized condition (Yi et al., 2014b), and validated against field
24 measurements for various locations in Alaska, the Arctic, and the QTP (Yi et al., 2009b, Yi et
25 al., 2013, Yi et al., 2014a).

26 **2.4 Model inputs and initialization**

27 We used the monthly averaged air temperature, downward radiation, precipitation and

1 humidity as input to drive the DOS-TEM. Leaf area index (LAI), leaf area per unit ground
2 surface area, was specified to be $0.6 \text{ m}^2\text{m}^{-2}$ in July and August, $0.1 \text{ m}^2\text{m}^{-2}$ in April and
3 October, $0 \text{ m}^2\text{m}^{-2}$ between November and March, and interpolated linearly in other months. It
4 is used in the DOS-TEM to calculate ground surface temperature in combination with other
5 meteorological variables (Yi et al., 2013). Its value is unchanged within each month.

6 Soil temperature and moisture were initialized at $-1 \text{ }^\circ\text{C}$ and saturation. The temperature
7 gradient at the bottom of bedrock was set to be $0.06 \text{ }^\circ\text{C cm}^{-1}$ based on borehole observations.
8 Volumetric unfrozen liquid water in winter was set to be 0.1 based on observations. Multi-
9 year (2003-2012) mean monthly driving data were used to spin up the model for 100 yr. In
10 this way, suitable initial values of soil moisture, temperature and rock temperature of each
11 layer are generated before driving DOS-TEM with monthly data over the period of 2003-2012.

12 **2.5 Sensitivity analyses**

13 The soil textures on the QTP mainly consist of loam, sand, and coarse fragment soils (Wu and
14 Nan, 2016). We used a uniform sand or loam soil profile to represent coarse and fine soil
15 textures, respectively. Sands are the most coarsest texture considered in most the modeling
16 studies (e.g. Oleson et al., 2010). Therefore, we used our measured parameters to substitute
17 the parameters of sand and loam to investigate the effects of coarse-fragment soil parameters
18 on permafrost dynamics. We first ran DOS-TEM using the default porosity, soil thermal
19 conductivity (Equation 4), hydraulic conductivity (Equation 8), and matric potential schemes
20 of these two default soil textures (Equation 7). The default parameters Φ , Ψ_{sat} , K_{sat} and B were
21 calculated based on soil texture used in Community Land Model (Equation 7 and 8; Oleson et
22 al., 2010). We then substituted the default values of Φ , Ψ_{sat} , K_{sat} and B based on our
23 laboratory measurements and calibration. Parameters Ψ_{sat} and B were fitted with measured
24 matric potential data using Isqcurvefit tools of Matlab. We did not calibrate soil thermal
25 conductivity to retrieve parameters of Equation 5 and 6. Instead, we interpolated measured
26 thermal conductivities over a range of degrees of saturation (0 to 1), which was used as a
27 lookup table by the DOS-TEM. Therefore, our sensitivity analyses considered a set of 4
28 factors, i.e. porosity, matric potential (Ψ_{sat} and B), hydraulic conductivity (K_{sat} and B) and
29 thermal conductivity. We also analyzed 3 different slopes (0, 5 and 10°) and 3 different soil
30 thicknesses (3.25, 4.25 and 5.25 m) above 56 m of bed rock. There were 11 soil layers with
31 the top 9 layers being 0.05, 0.1, 0.1, 0.2, 0.2, 0.2, 0.3, 0.3 and 0.3 m thick. The thicknesses of

1 the bottom 2 soil layers were 0.5 and 1 m, 0.5 and 2 m, and 1.5 and 2 m for the 3.25, 4.25 and
2 5.25 m cases, respectively. There were 6 rock layers with thicknesses of 2, 2, 4, 8, 16 and 20
3 m. Since the site is on the top of upland plain landforms, we did not further test the effects of
4 aspect on radiation on ground surface. We instead considered the effects of slope on surface
5 runoff. In summary, our sensitivity analyses with the DOS-TEM involved 288 different
6 combinations of parameter values.

7 We did not measure the heat capacity. The maximum and minimum heat capacities of mineral
8 soil types considered in land surface model are 2.355 and 2.136 MJ m⁻³, respectively, giving a
9 relative difference less than 10%. Therefore, in this study, we did not make sensitivity tests
10 using thermal diffusivity (the ratio between thermal conductivity and heat capacity).

11 **3 Results**

12 **3.1 Soil physical properties**

13 **3.1.1 Soil porosity, particle size and bulk density**

14 Results from laboratory analysis of the soil samples are shown in Table 1 and 2. The mean
15 weight of the coarse soil fraction (particle size diameter > 2 mm) of different soil layers
16 ranged from 0.38 to 0.65 with a mean of 0.55. According to the USDA classification system
17 (clay (<2 μ m), silt (2 –50 μ m, in this study 2-63 μ m) and sand (50 μ m -2.0 mm, in this
18 study 63 μ m -2.0 mm)), the major soil texture of this site was loamy sand, with the exception
19 of sandy loam at depth of 20-30 cm. The default porosities of sand and loam were 37.3% and
20 43.5%, respectively. The measured porosity of samples down to 2 m depth ranged from 21%
21 to 30% with a mean of 27%, and the mean bulk density ranged from 1.61 to 1.86 g cm⁻³ with a
22 mean of 1.74 g cm⁻³. The porosity calculated from bulk density (= 1- bulk density/2.65 g cm⁻³)
23 ranged from 29.8% to 39.2%. No significant relationships were found among soil porosity,
24 bulk density and the coarse soil fraction (p>0.05).

25 **3.1.2 Thermal conductivity**

26 The results of the thermal conductivity determinations are shown in Table 3. The unfrozen
27 dry soil thermal conductivity of different soil layers ranged from 0.24 to 0.40 W m⁻¹ K⁻¹ with
28 a mean of 0.36 W m⁻¹ K⁻¹, and the frozen dry soil thermal conductivity ranged from 0.25 to

1 0.41 W m⁻¹ K⁻¹ with a mean of 0.35 W m⁻¹ K⁻¹. The difference of dry thermal conductivity
2 between frozen and unfrozen states was small. The unfrozen saturated soil thermal
3 conductivity of different soil layers ranged from 2.15 to 2.74 W m⁻¹ K⁻¹ with a mean of 2.48
4 W m⁻¹ K⁻¹. The frozen saturated soil thermal conductivity ranged from 3.06 to 3.72 W m⁻¹ K⁻¹
5 with a mean of 3.33 W m⁻¹ K⁻¹. The difference of saturated thermal conductivity between
6 frozen and unfrozen states was about 0.85 W m⁻¹ K⁻¹. There existed a threshold of soil
7 wetness (i.e. ~0.28 m³ m⁻³), below which frozen soil thermal conductivity was slightly smaller
8 than unfrozen soil (Figure 4a).

9 Results from determining thermal conductivities using the Côté and Konrad (2005) scheme
10 are shown in Figure 4b. The default dry frozen and unfrozen thermal conductivities for sand
11 and loam were about 0.42 and 0.24 W m⁻¹ K⁻¹, respectively. The saturated frozen and
12 unfrozen thermal conductivities of sand were 3.11 and 1.90 W m⁻¹ K⁻¹, respectively. Those of
13 loam were about 2.36 and 1.33 W m⁻¹ K⁻¹, respectively. Results from determining thermal
14 conductivities using the Farouki (1986) scheme are shown in Figure 4c. The default dry
15 frozen and unfrozen thermal conductivities for sand and loam were about 0.97 and 0.63 W m⁻¹
16 K⁻¹, respectively. The saturated frozen and unfrozen thermal conductivities of sand were
17 5.21 and 3.18 W m⁻¹ K⁻¹, respectively. Those of loam were about 4.49 and 2.52 W m⁻¹ K⁻¹,
18 respectively.

19 **3.1.3 Saturated hydraulic conductivity**

20 The mean saturated hydraulic conductivity of soil layers, shown in Table 4, ranged from
21 0.0036 to 0.0315 mm s⁻¹. The maximum saturated hydraulic conductivity was about 8.7 times
22 larger than the minimum. The saturated hydraulic conductivity tended to be larger with
23 increasing proportion of coarse fragment in the soil samples (Figure 5a), and was about 0.03-
24 0.06 mm s⁻¹ for some samples with coarse fragment greater than 70%. The default saturated
25 hydraulic conductivities of sand and loam were 0.024 and 0.0042 mm s⁻¹, respectively.

26 **3.1.4 Matric potential**

27 The correlation coefficients between calculated and fitted matric potential, shown in Table 4,
28 were all greater than 0.96. The mean absolute value of saturated matric potential of soil layers
29 ranged from 14.47 to 603.7 mm, and those of B ranged from 1.89 to 5.22 (Table 4 and Figure

1 5b). The default absolute value of saturated matric potential of sand and loam were 47.29 and
2 207.34 mm, respectively, and the B values 3.39 and 5.77, respectively.

3 **3.2 Comparisons between simulations using default vs. measured parameters**

4 **3.2.1 Soil temperature**

5 The mean root mean squared errors (RMSEs) between monthly measured soil temperatures
6 and model runs with measured parameters using different combination of soil thicknesses
7 (3.25, 4.25 and 5.25 m) and slopes (0, 5 and 10°) were about 1.07 °C at 20 cm (Figure 6c).
8 The mean RMSEs for all model runs with default sand and loam parameters were about 0.97
9 and 1.18 °C, respectively. For other soil layers, the RMSEs of model runs with measured
10 parameters were much smaller than those with default sand and loam parameters (Figures 6d-
11 l). The simulated soil temperatures using default sand and loam parameters were all lower
12 than measured ones in summer at 100 and 200 cm; and in winter at 400 cm. The RMSEs can
13 be as large as 2.53 °C (Figure 6e).

14 The standard deviations of soil temperatures among different slopes and soil thicknesses
15 using measured parameters were larger than those using the default parameters (Figure 6); and
16 they increased from 0.40 °C at 100 cm to 0.61 °C at 200 cm (Figure 6f and i). The standard
17 deviations using default loam parameters were smaller (<0.15 °C at all depths) than those
18 using default sand parameters.

19 **3.2.2 Soil liquid water**

20 The mean RMSEs between monthly measured liquid soil volumetric water content (VWC)
21 and model simulations with measured parameters ranged from 0.03 to 0.09, which were
22 smaller than RMSEs for sand and loam parameters (Figure 7). The model simulations for
23 loam parameters have larger RMSEs than those for sand parameters. VWCs were always
24 overestimated in warm seasons at depths of 10, 40 and 80 cm. VWCs were underestimated at
25 a depth of 160 cm, where the simulated soil was frozen. All model simulations overestimated
26 VWC at 40 cm, where the maximum measured VWCs were about 0.1 (Figure 7d-f).

27 The standard deviations of VWC among different slopes and soil thicknesses using sand
28 parameters were about 0.077, which were larger than those using measured parameters

1 (~0.062). The standard deviations of VWC using loam parameters (<0.032) were less than
2 those using measured parameters.

3 **3.2.3 Active layer depth (ALD)**

4 The mean RMSEs between measured ALDs (derived from linear interpolation of soil
5 temperatures) and modelled ALDs (simulated explicitly) were about 1.06, 1.72 and 0.28 m for
6 model runs with sand, loam and measured parameters (Figure 8a). The mean standard
7 deviations were about 0.088, 0.026 and 0.28 m. All simulations using sand and loam
8 parameters underestimated ALDs.

9 **3.2.4 Permafrost lower boundary (PLB)**

10 The mean RMSEs between measured PLBs (derived from linear interpolation of temperatures)
11 and modelled PLBs (derived from linear interpolation of simulated bed rock temperatures)
12 were about 10.25, 10.23 and 6.71 m for model runs with sand, loam and measured parameters
13 (Figure 6b). The mean standard deviations were about 1.89, 1.51 and 6.62 m. All simulations
14 using sand and loam parameters overestimated PLBs.

15 **3.3 Model sensitivity analyses**

16 Deep soil layers used in models are usually specified as being thick. For example, a 1 m thick
17 soil layer was used in our simulations starting around 3 m soil depth. Soil temperatures at this
18 depth are usually close to 0°C. Therefore, the RMSEs of deep soil layers were small and did
19 not facilitate evaluation of model sensitivities. In the following subsections, we used 20 and
20 100 cm soil temperatures, ALDs and PLBs for sensitivity analysis.

21 **3.3.1 Effects of single parameter sensitivity analyses**

22 **Porosity**

23 Replacing default sand or loam porosity with measured porosities changed mean RMSEs of
24 soil temperatures (model runs with 3 different slopes and 3 different soil thicknesses at 2
25 different soil depths) from 1.18 or 1.84 °C to 1.25 or 1.09 °C, respectively (Figure 9 and 10).
26 Mean RMSEs of ALD were reduced from 1.06 or 1.72 m to 0.22 or 0.85 m, respectively.
27 Mean RMSEs of PLB were changed from 10.26 or 10.24 m to 6.61 or 10.97 m. Mean

1 RMSEs of VWC were reduced from 0.074 or 0.14 to 0.06 or 0.062 when measured porosities
2 were used for replacing default sand or loam porosity, respectively (Figure 11 and 12).

3 **Thermal conductivity**

4 Replacing default sand or loam thermal conductivity with measured thermal conductivity
5 reduced mean RMSEs of soil temperatures from 1.18 or 1.84°C to 1.02 or 1.15°C,
6 respectively (Figure 9 and 10). Mean RMSEs of ALD were reduced from 1.06 or 1.72 m to
7 0.56 or 1.04 m, respectively. Mean RMSEs of PLB were changed from 10.26 or 10.24 m to
8 4.18 or 1.27 m, respectively. Mean RMSEs of VWC changed very slightly (Figure 11 and 12).

9 **Hydraulic conductivity and matric potential**

10 Replacing default sand or loam hydraulic conductivity with measured parameters had very
11 small effects on mean RMSEs of soil temperatures and ALDs (Figure 9 and 10). The same
12 was true for matric potential. When hydraulic conductivity of default sand or loam was
13 substituted, mean RMSEs of PLB decreased or increased, respectively. However, when
14 matric potential was substituted, mean RMSEs of PLBs increased or decreased, respectively.
15 When hydraulic conductivity or matric potential parameters were substituted in default sand
16 or loam parameters, mean RMSEs of VWC changed slightly (Figure 11 and 12).

17 **3.3.2 Effects of combined parameters**

18 We compared model simulations with different combinations of measured parameters
19 (porosity, thermal conductivity, hydraulic conductivity and matric potential) to those with one
20 substituted measured parameter. We ranked those model runs with less RMSEs than the best
21 of the model runs with one parameter substituted with a measurement-derived value (Table 5
22 and 6). We didn't consider the 10 cm soil temperature, which were similar among all model
23 runs.

24 For sand, model simulations with porosity and thermal conductivity or hydraulic
25 conductivity substituted had 4 outcomes with lower RMSEs (Table 5 and Figures 9 and 11).
26 Only 2 out of 7 outcomes had lower RMSEs with all 4 parameters substituted. Among all the
27 18 cases with RMSEs less than the individual "best" RMSE, porosity was included 18 times,
28 followed by thermal conductivity and hydraulic conductivity both with 10 times.

29 For loam, model simulations with porosity and thermal conductivity substituted had 5
30 outcomes with lower RMSEs (Table 6 and Figures 10 and 12). Among all the 27 cases with

1 RMSEs less than the individual “best” RMSE, porosity was included 27 times, followed by
2 thermal conductivity with 16 times, and matric potential with 14 times.

3 **3.3.3 Effects of slope and soil thickness**

4 Changes of slope alone had small effects on simulated soil temperatures and ALDs (Figures 9
5 and 10). An increase of slope generally reduced RMSEs of VWCs (Figures 11 and 12). Model
6 simulations with porosity substituted had smaller differences in VWC RMSE between
7 different cases of slopes. For example, the mean RMSEs of model simulations with slopes of
8 0° or 5° and sand parameters substituted with measured porosity were 0.078 or 0.048,
9 respectively. While those with porosity not substituted were 0.141 or 0.055, respectively.
10 Similarly, the mean RMSEs of model simulations using default loam parameters with
11 porosity substituted were 0.08 or 0.05 for slope of 0° or 5° , respectively. The mean RMSEs
12 were 0.18 or 0.1 with porosity not substituted, respectively. For a further increase of slope to
13 10° , changes of RMSEs of VWCs at depths of 10-160 cm were small.

14 Soil thickness had small effects on 20 and 100 cm soil temperatures and 10-160 cm VWCs,
15 and it had prominent effects on PLB for a few cases only with a slope of 10° (Figures 9 and
16 10).

17 **4 Discussion**

18 **4.1 Characteristics of soil physical properties**

19 Although the effects of coarse fragment soil on permafrost dynamics have been considered in
20 a few modelling studies, the thermal and hydraulic properties of coarse fragment soil were
21 calculated without validation or calibration (Pan et al., 2017; Wu et al., 2018). To our
22 knowledge, this is the first study measuring physical properties of coarse fragment soil
23 samples from permafrost region of the QTP.

24 The weight fraction of coarse fragment (diameter > 2mm, including gravel) in the soil
25 samples we analysed was greater than 55% on average. While the typical soil types
26 considered in land surface models and other models usually have much smaller diameter. For
27 comparison, the fractions of gravel considered in Pan et al. (2017) ranges from 5% to 33%
28 and from 10% to 28% for the Madoi and Naqu sites, respectively. The Beiluhe site and the
29 aforementioned sites are located in regions with Gelisols and Inceptisols, which occupy ~62%

1 of the permafrost regions of the QTP (Li et al., 2015). It is possible that coarse fragment soil
2 commonly exists on the QTP. The dataset of Wu and Nan (2016) indicated that gravel content
3 widely exists on the middle and western part of the QTP. The saturated hydraulic conductivity
4 and matric potential of soil samples measured in this study were more similar to sand than to
5 loam (see Section 3.1). It is consistent with the study of Wang et al. (2013) that coarse soil
6 material has poor water holding capability.

7 The measured thermal conductivities of saturated soil samples were relatively close to
8 those estimated by the Côté and Konrad (2005) scheme. But they were much less than those
9 estimated by the Farouki scheme (Figure 4). Several other studies also found that Farouki
10 scheme overestimated soil thermal conductivity (Chen et al. 2012; Luo et al., 2009).

11 One important finding of this study is the relatively small value of porosity. The measured
12 porosity ranged from 0.206 to 0.302, which is less than those of soil types considered in land
13 surface models. For example, the porosities of mineral soil types considered in Community
14 Land Model range from 0.37 to 0.48 (Oleson et al., 2010). Porosity determines the maximum
15 water stored in a soil layer, and affects soil thermal conductivity, hydraulic conductivity and
16 matric potential (Equation 5-8). It plays a more important role than other parameters in
17 simulated soil thermal and hydrological dynamics (Table 5 and 6; Figure 9-12). It is
18 noteworthy that it is easy and efficient to measure porosity.

19 **4.2 Effects of soil water on permafrost dynamics**

20 Soil water not only affects soil thermal properties (e.g. thermal conductivity and heat
21 capacity), but also affects the amount of latent heat lost or gained, for freezing or thawing,
22 respectively (Goodrich, 1978; Farouki, 1986). Soil water is determined by infiltration,
23 evapotranspiration, water movement among soil layers, subsurface runoff and exchange with
24 a water reservoir. Therefore, processes or parameters that affect soil water dynamics will also
25 affect permafrost dynamics. This study quantitatively assessed the effects of soil water on
26 permafrost dynamics. For example, when default loam parameters with high porosity and low
27 saturated hydraulic conductivity were used, soil layers were almost saturated (Figure 7). The
28 simulated ALDs were about 1.58 m, which was less than half of measured ALDs (Figure 8a).
29 When the slope was 0°, subsurface runoff didn't occur in the saturated zone above the bottom
30 of the active layer. The simulated soil water content was generally higher in the active layer.
31 However, when the slope was 5°, the simulated soil water content was less and the RMSE was

1 smaller (Figure 11 and 12). These patterns were especially obvious when both porosity and
2 saturated hydraulic conductivity were large (Equation 9; Figure 11 and 12). Other studies
3 have also emphasized the importance of subsurface runoff above the bottom of the active
4 layer (Frey and McClelland, 2009; Walvoord and Striegl, 2007). The effects of soil water
5 content on soil thermal dynamics increased with soil and rock depth (Figure 9 and 10). The
6 biggest effects were on PLB, which became manifest during long-term spinup procedures.

7 Land surface models generally represent soil water dynamics (e.g. Chen et al., 2015;
8 Oleson et al., 2010; Wang et al., 2017). However, the thermal processes in permafrost models
9 usually use specified thermal properties, which were static during model simulations (Li et al.,
10 2009; Nan et al., 2005; Qin et al., 2017; Zou et al., 2017). As shown in this study, soil thermal
11 and hydrological properties depend largely on soil water content. It is critical to simulate soil
12 water dynamics to properly project permafrost dynamics in the future.

13 **4.3 Limitations and Outlook**

14 **4.3.1 Sampling and laboratory measurement**

15 We used cut rings with 10 cm diameter to sample soil and weathered mudstones. However, it
16 is very likely that there could have been much bigger coarse fragment soils. Therefore, larger
17 containers should be used to take samples for further laboratory analysis in the future.

18 During our laboratory work, we found two phenomena. First, we originally used the QL-
19 30 thermophysical instrument (Anter Corporation, US) to measure thermal conductivity. It
20 worked properly under unfrozen condition. However, when frozen, the surface of the soil
21 sample was usually uneven due to frost heave, which reduces the contact between the QL-30
22 plate and the soil sample surface. The measured frozen thermal conductivities were smaller
23 than unfrozen thermal conductivity even for the case of saturation, which were definitely
24 wrong, thus we used the KD2 pro to determine thermal conductivities. The second
25 phenomenon was that there seems to be a threshold of soil wetness, below which unfrozen
26 soil thermal conductivity is greater than frozen soil thermal conductivity (Figure 4a). This
27 pattern was somewhat exhibited in estimates of the Côté and Konrad (2005) scheme (Figure
28 4b), but not in the estimates of the Farouki scheme (Figure 4c). More measurements using
29 instruments with higher accuracy should be made in the future.

1 It is ideal to draw water in soil samples under a vacuum condition before weighing dry
2 soil sample. Unfortunately, we do not have such instrument. We dried soil samples in an oven
3 at 65 °C for over 48 h, which is commonly used in ecological studies, e.g. Qin et al. (2018).
4 The measured porosities are generally smaller than those calculated from bulk density. We
5 made additional model simulations using porosities calculated from bulk density in
6 combination with other measured parameters. Results showed that the RMSEs of ALD and
7 PLB were 0.55 m and 4.78 m, respectively (Figures not shown). While those used measured
8 porosities were 0.28 m and 6.71 m. Considering the importance of porosity on simulated
9 permafrost dynamics, it is important to draw water out of soil samples in a vacuum condition
10 before weighing dry soil samples in the future.

11 **4.3.2 Model simulation**

12 Although the DOS-TEM using measured parameters provided satisfactory results, there are
13 some aspects requiring further improvement in the future. For example, the measured soil
14 moistures at 40 cm depth were less than $0.1 \text{ m}^3 \text{ m}^{-3}$. However, the simulated soil moistures
15 were always much greater (Figure 7f). There were also spikes in measured soil moistures at
16 80 and 160 cm depths, which were not presented in the simulation (Figure 7 i and l). In the
17 DOS-TEM, the unfrozen soil water content, or supercold water, was prescribed to be 0.1
18 m^3/m^3 . When soil is freezing, if soil liquid water content is less than this value, no phase
19 change will happen (Figure 7k). Therefore, model results would improve with the capability
20 to simulate the dynamics of unfrozen soil water content (Romanovsky and Osterkamp, 2000).

21 **4.3.3 Regional applications**

22 Soil texture plays an important role in permafrost dynamics (Figure 8). However, the
23 dominant soil texture on the QTP from Wu and Nan (2016) are loam, sand, and gravel. The
24 specification of loam in simulations results in estimates of ALD that are much smaller than
25 measurements (Yi et al., 2014a). To properly simulate the distribution and dynamics of
26 permafrost on the QTP under climate change scenarios, it is important to develop proper
27 schemes of soil physical properties in relation to coarse fragment content (including gravel)
28 and to develop regional datasets of soil texture for input. Coarse fragment content affects soil
29 physical properties. For example, soil porosity and saturated hydraulic conductivity are
30 determined by the fraction of gravel, diameter and degree of mixture (Zhang et al., 2011).

1 Organic soil carbon content in mineral soil on the QTP affects soil porosity and thermal
2 conductivity (Chen et al., 2012). In the site considered in this study, the amount of organic
3 soil carbon in soil was small (Figure 2), and we did not consider the effects of organic soil
4 carbon on soil properties explicitly. Alpine swamp meadow, alpine meadow, alpine steppe
5 and alpine desert are the major vegetation types on the QTP (Wang et al., 2016; see also
6 Figure 1b). Alpine swamp meadow and alpine meadow usually contain fine soil particles and
7 high organic carbon density; while the other two types usually contain coarse soil particle and
8 low organic carbon density (Qin et al., 2015). More laboratory work is needed to develop
9 proper schemes for representing mixed soil with fine mineral, coarse fragment (including
10 gravel) and organic carbon in permafrost models. It is the first priority to develop schemes
11 that make use of porosity data sets, due to its importance and simplicity of measurement.

12 The development of a spatially explicit dataset of soil texture is also required for regional
13 applications of projecting permafrost changes on the QTP. One way is to collect relevant data
14 through extensive field campaigns (e.g., Li et al., 2015). Currently, gravelly soil has only been
15 mentioned in scientific literature on the QTP (Chen et al., 2015; Wang et al., 2011; Yang et al.,
16 2009). Only recently, a preliminary dataset considering gravel has been created (Wu and Nan,
17 2016). Ground penetrating radar is a feasible tool to retrieve soil thickness above the coarse
18 fragment soil layer (Han et al., 2016). Aerial photos taken with unmanned aerial vehicles have
19 been used recently to identify coarse fragment soil (Chen et al., 2017; Yi 2017). In
20 combination with ancillary datasets (e.g. geomorphology, topography, vegetation), it is
21 possible to improve the accuracy of spatial datasets of soil texture on the QTP (Li et al., 2015;
22 Wu et al., 2016). Another way is to retrieve soil physical properties using data assimilation
23 technology, such as Yang et al. (2016) who assimilated porosity using a land surface model
24 and microwave data.

25 **5 Conclusions**

26 In this study, we excavated soil samples from a permafrost site on the central QTP and
27 measured soil physical properties in laboratory. Coarse fragment soil was common in the soil
28 profile and porosity was much smaller than the typical soil types used in land surface models.
29 We then performed sensitivity analysis of these parameters on soil thermal and hydrological
30 processes within a terrestrial ecosystem model. When default sand or loam parameters were
31 substituted with measured soil properties, the model errors of soil temperature, soil liquid

1 water content, active layer depth and permafrost low boundary were generally reduced.
2 Sensitivity analyses showed that porosity played a more important role in reducing model
3 errors than other soil properties examined. Though it is unclear how representative this soil is
4 in the QTP, it is clear that soil physical properties specific to the QTP should be used to
5 properly project permafrost dynamics into the future.

6 *Acknowledgements.* We would like to thank Prof. Dave McGuire of University of Alaska
7 Fairbanks for his careful editing; Dr. Yi Sun for vegetation classification; Dr. Xia Cui of
8 Lanzhou University, Mr. Guangyue Liu for determining depth of zero annual amplitude and
9 Mr. Yan Qin for measurements of soil particle size distribution; Prof. Chien-Lu Ping of
10 University of Alaska and Dr. Wangping Li of Lanzhou University of Technology for helping
11 on soil taxonomy; and the editor and two anonymous reviewers for valuable comments. This
12 study was jointly supported through grants provided as part of the National Natural Science
13 Foundation Commission (41422102, 41730751 and 41690142).

14 **References**

- 15 Anisimov, O. A.: Potential feedback of thawing permafrost to the global climate system
16 through methane emission, *Environ. Res. Lett.*, 2, 045016, doi:10.1088/1748-
17 9326/2/4/045016, 2007.
- 18 Arocena, J., K. Hall, and L.P.: Soil formation in high elevation and permafrost areas in
19 the Qinghai Plateau (China), *Spanish Journal of Soil Sciences*, 2, 34-49, 2012.
- 20 Azam, G., Grant, C. D., Murray, R. S., Nuberg, I. K., and Misra, R. K. : Comparison of the
21 penetration of primary and lateral roots of pea and different tree seedlings growing in
22 hard soils. *Soil Research*, 52, 87-96, 2014.
- 23 Boike, J., Kattenstroth, B., Abramova, E., Bornemann, N., Chetverova, A., Fedorova, I., and
24 Langer, M.: Baseline characteristics of climate, permafrost and land cover from a new
25 permafrost observatory in the Lena River Delta, Siberia (1998-2011), *Biogeosciences*
26 (BG), 10, 2105-2128, 2013.
- 27 Chen, H., Nan, Z., Zhao, L., Ding, Y., Chen, J., & Pang, Q.: Noah Modelling of the
28 Permafrost Distribution and Characteristics in the West Kunlun Area, Qinghai-Tibet
29 Plateau, China. *Permafrost Periglac*, 26, 160-174, 2015.

- 1 Chen, J., Yi, S., and Qin, Y.: The contribution of plateau pika disturbance and erosion on
2 patchy alpine grassland soil on the Qinghai-Tibetan Plateau: Implications for grassland
3 restoration. *Geoderma*, 297, 1-9, 2017.
- 4 Chen, Y., Yang, K., Tang, W., Qin, J., and Zhao, L.: Parameterizing soil organic carbon's
5 impacts on soil porosity and thermal parameters for Eastern Tibet grasslands, *Science in*
6 *China Series D: Earth Sciences (EN)*, 55, 1001-1011, 2012.
- 7 Cote, J. and J. Konrad: A generalized thermal conductivity model for soils and construction
8 materials, *Can. Geotech. J.*, 42, 443-458, 2005.
- 9 Du, Z., Y. Cai, Y. Yan, and X. Wang: Embedded rock fragments affect alpine steppe plant
10 growth, soil carbon and nitrogen in the northern Tibetan Plateau, *Plant Soil*, 420, 79-92,
11 2017.
- 12 Farouki, O. T.: Thermal properties of soils, *Cold Reg. Res. and Eng. Lab.*, Hanover, N. H,
13 1986.
- 14 Fox, J. D.: Incorporating Freeze-Thaw Calculations into a water balance model, *Water Resour.*
15 *Res.*, 28, 2229-2244, 1992.
- 16 Frey, K. E., and McClelland, J. W.: Impacts of permafrost degradation on arctic river
17 biogeochemistry, *Hydrol. Process*, 23, 169-182, 2009.
- 18 Goodrich, E. L.: Efficient Numerical Technique for one-dimensional Thermal Problems with
19 phase change, *Int. J. Heat Mass Transfer*, 21, 615-621, 1978.
- 20 Gwenzi, W., Hinz, C., Holmes, K., Phillips, I. R., and Mullins, I. J.: Field-scale spatial
21 variability of saturated hydraulic conductivity on a recently constructed artificial
22 ecosystem, *Geoderma*, 166, 43-56, 2011.
- 23 Han, X., Liu, J., Zhang, J., and Zhang, Z.: Identifying soil structure along headwater
24 hillslopes using ground penetrating radar based technique. *Journal of Mountain*
25 *Science*, 13, 405-415, 2016.
- 26 Jorgenson, M. T., Shur, Y. L., and Pullman, E. R.: Abrupt increase in permafrost degradation
27 in Arctic Alaska, *Res. Lett.*, 33, L02503, doi:10.1029/2005GL024960, 2006.
- 28 Langer, M., Westermann, S., Heikenfeld, M., Dorn, W., and Boike, J.: Satellite-based
29 modeling of permafrost temperatures in a tundra lowland landscape, *Remote Sensing of*
30 *Environment*, 135, 12-24, 2013.
- 31 Li, J., Sheng, Y., Wu, J., Chen, J., and Zhang, X.: Probability distribution of permafrost along
32 a transportation corridor in the northeastern Qinghai province of China. *Cold Regions*
33 *Science and Technology*, 59, 12-18, 2009.

- 1 Li, W., L. Zhao, X. Wu, Y. Zhao, H. Fang, and W. Shi: Distribution of soils and landform
2 relationships in the permafrost regions of Qinghai-Xizang (Tibetan) Plateau, Chinese Sci.
3 Bull., 23, 2216-2226, 2015.
- 4 Lin, Z., F. Niu, H. Liu, and J. Lu: Hydrothermal processes of alpine tundra lakes, Beiluhe
5 Basin, Qinghai-Tibet Plateau, Cold Reg. Sci. Techol., 65, 446-455, 2011.
- 6 Luo, S., Lv, S., Zhang, Y., Hu, Z., Ma, Y., Li, S., and Shang, L.: Soil thermal conductivity
7 parameterization establishment and application in numerical model of central Tibetan
8 Plateau, Chinese Journal of Geophysics, 52, 919-928, 2009. (in Chinese with English
9 Abstract)
- 10 McGuire, A. D., J. Melillo, E. G. Jobbagy, D. Kicklighter, A. L. Grace, B. Moore, and C. J.
11 Vorosmarty: Interactions Between Carbon and Nitrogen Dynamics in Estimating Net
12 Primary Productivity for Potential Vegetation in North America, Global Biogeochem. Cy.,
13 6(2), 101-124, 1992.
- 14 McGuire, A. D., J. S. Clein, J. Melillo, D. Kicklighter, R. A. Meier, C. J. Vorosmarty, and M.
15 C. Serreze: Modelling carbon responses of tundra ecosystems to historical and projected
16 climate: sensitivity of pan-Arctic carbon storage to temporal and spatial variation in
17 climate, Global Change Biol., 6 (Suppl. 1), 141-159, 2000.
- 18 McGuire, A. D., Anderson, L. G., Christensen, T. R., Dallimore, S., Guo, L., Hayes, D. J., .
19 and Roulet, N.: Sensitivity of the carbon cycle in the Arctic to climate change. Ecological
20 Monographs, 79, 523-555, 2009.
- 21 Nan, Z., Li, S., and Cheng, G.: Prediction of permafrost distribution on the Qinghai-Tibet
22 Plateau in the next 50 and 100 years. Science in China Series D: Earth Sciences, 48, 797-
23 804, 2005.
- 24 Nelson, F. E., Anisimov, O. A., and Shiklomanov, N. I.: Subsidence risk from thawing
25 permafrost, Nature, 410(6831), 889-890, 2001.
- 26 Oleson, K. W., Lawrence, D. M., Bonan, G. B., Flanner, M. G., Kluzek, E., Lawrence, P. J.,
27 Levis, S., Swenson, S. C., and Thornton, P.: Technical description of version 4.0 of the
28 Community Land Model (CLM), University Corporation for Atmospheric Research,
29 NCAR 2153-2400, 2010.
- 30 Pan, Y., S. Lv, S. Li, Y. Gao, X. Meng, Y. Ao, and S. Wang: Simulating the role of gravel in
31 freeze-thaw process on the Qinghai-Tibet Plateau, Theor. Appl. Climatol., 127, 1011-
32 1022, 2017.

- 1 Qin, Y., J. E. Hiller, G. Jiang, and T. Bao: Sensitivity of thermal parameters affecting cold-
2 region ground-temperature predictions, *Environ. Earth Sci.*, 68, 1757-1772, 2013.
- 3 Qin, Y., Yi, S., Chen, J., Ren, S., and Ding, Y.: Effects of gravel on soil and vegetation
4 properties of alpine grassland on the Qinghai-Tibetan plateau. *Ecological Engineering*, 74,
5 351-355, 2015.
- 6 Qin Y., Wu, T. , Zhao, L., Wu, X., Li, R., Xie, C., Pang, Q., Hu, G., Qiao, Y., Zhao, G., Liu,
7 G., Zhu, X., and Hao, J.: Numerical Modeling of the Active Layer Thickness and
8 Permafrost Thermal State Across Qinghai-Tibetan Plateau, *Journal of Geophysical*
9 *Research: Atmospheres*, doi:10.1002/2017JD026858, 2017.
- 10 Qin, Y., S. Yi, Y. Ding, G. Xu, J. Chen, and Z. Wang: Effects of small-scale patchiness of
11 alpine grassland on ecosystem carbon and nitrogen accumulation and estimation in
12 northeastern Qinghai-Tibetan Plateau, *Geoderma*, 318, 52-63, 2018.
- 13 Romanovsky, V. E. and T. E. Osterkamp: Effects of unfrozen water on heat and mass
14 transport processes in the active layer and permafrost, *Permafrost Periglac.*, 11, 219-239,
15 2000.
- 16 Salmon, V. G., Soucy, P., Mauritz, M., Celis, G., Natali, S. M., Mack, M. C., and Schuur, E.
17 A.: Nitrogen availability increases in a tundra ecosystem during five years of
18 experimental permafrost thaw, *Global Change Biol.*, 22, 1927-1941, 2016.
- 19 Soil Survey Staff. *Keys to Soil Taxonomy*, 12th ed. USDA-Natural Resources Conservation
20 Service, Washington, DC, 2014.
- 21 Swenson, S. C., D. M. Lawrence, and H. Lee: Improved simulation of the terrestrial
22 hydrological cycle in permafrost regions by the Community Land Model, *Journal of*
23 *Advances in Modeling Earth Systems*, 4, M08002, doi:10.1029/2012MS000165, 2013.
- 24 Walvoord, M. A., and Striegl, R. G.: Increased groundwater to stream discharge from
25 permafrost thawing in the Yukon River basin: Potential impacts on lateral export of
26 carbon and nitrogen. *Geophys. Res. Lett.*, 34, L12402, doi:10.1029/2007GL030216, 2007.
- 27 Wang, F. X., Kang, Y., Liu, S. P., and Hou, X. Y.: Effects of soil matric potential on potato
28 growth under drip irrigation in the North China Plain. *Agricultural water management*, 88,
29 34-42, 2007.
- 30 Wang, G., Li. Y., Wang. Y., and Wu, Q.: Effects of permafrost thawing on vegetation and soil
31 carbon pool losses on the Qinghai-Tibet Plateau, China, *Geoderma*, 143, 143-152,2008.
- 32

- 1 Wang, H., B. Xiao, M. Wang, and Ming'an Shao: Modeling the soil water retention curves of
2 soil-gravel mixtures with regression method on the Loess Plateau of China, PLoS ONE, 8,
3 e59475, doi:10.1371/journal.pone.0059475, 2013.
- 4 Wang, L., Zhou, J., Qi, J., Sun, L., Yang, K., Tian, L., and Koike, T.: Development of a land
5 surface model with coupled snow and frozen soil physics, Water Resources Research, 53,
6 5085-5103, doi:10.1002/2017WR020451, 2017.
- 7 Wang, X., Liu, G., and Liu, S.: Effects of gravel on grassland soil carbon and nitrogen in the
8 arid regions of the Tibetan Plateau. Geoderma, 166, 181-188, 2011.
- 9 Wang, Z., Q. Wang, L. Zhao, X. Wu, G. Yue, D. Zou, Z. Nan, G. Liu, Q. Pang, H. Fang, T.
10 Wu, J. Shi, K. Jiao, Y. Zhao, and L. Zhang: Mapping the vegetation distribution of the
11 permafrost zone on the Qinghai-Tibet Plateau, Journal of Mountain Sciences, 13, 1035-
12 1046, 2016.
- 13 Woo, M. K., Arain, M. A., Mollinga, M., and Yi, S.: A two-directional freeze and thaw
14 algorithm for hydrologic and land surface modelling. Geophys. Res. Lett., 31, L12501,
15 doi:10.1029/2004GL019475, 2004.
- 16 Wright, N., Hayashi, M., and Quinton, W. L.: Spatial and temporal variations in active layer
17 thawing and their implication on runoff generation in peat-covered permafrost
18 terrain. Water Resour. Res., 45, W05414, doi:10.1029/2008WR006880, 2009.
- 19 Wu, Q., Cheng, G., and Ma, W.: Impact of permafrost change on the Qinghai-Tibet Railroad
20 engineering. Science in China Series D: Earth Sciences, 47, 122-130, 2004.
- 21 Wu, Q., and Zhang, T.: Changes in active layer thickness over the Qinghai-Tibetan Plateau
22 from 1995 to 2007. J. Geophys. Res., 115, D09107, doi:10.1029/2009JD012974, 2010.
- 23 Wu, Q., Z. Zhang, S. Gao, and W. Ma: Thermal impacts of engineering activities and
24 vegetation layer on permafrost in different alpine ecosystems of the Qinghai-Tibet
25 Plateau, China, The Cryosphere, 10, 1695-1706, 2016.
- 26 Wu, X., Zhao, L., Fang, H., Zhao, Y., Smoak, J. M., Pang, Q., and Ding, Y.: Environmental
27 controls on soil organic carbon and nitrogen stocks in the high-altitude arid western
28 Qinghai-Tibetan Plateau permafrost region, J. Geophys. Res., 121, 176-187, 2016.
- 29 Wu, X. and Nan, Z.: A Multilayer Soil Texture Dataset for Permafrost Modeling over
30 Qinghai–Tibetan Plateau, IGARSS, 4917-4920, 2016

31

- 1 Wu, X., Z. Nan, S. Zhao, L. Zhao, and G. Cheng: Spatial modeling of permafrost distribution
2 and properties on the Qinghai-Tibetan Plateau, *Permafrost Periglac.*, DOI:
3 10.1002/ppp.1971, 2018
- 4 Yang, J., Mi, R., and Liu, J.: Variations in soil properties and their effect on subsurface
5 biomass distribution in four alpine meadows of the hinterland of the Tibetan Plateau of
6 China, *Environ. Geol.*, 57, 1881-1891, 2009.
- 7 Yang, K., Zhu, L., Chen, Y., Zhao, L., Qin, J., Lu, H., . and Fang, N.: Land surface model
8 calibration through microwave data assimilation for improving soil moisture
9 simulations, *Journal of Hydrology*, 533, 266-276, 2016.
- 10 Ye, B., Yang, D., Zhang, Z., and Kane, D. L.: Variation of hydrological regime with
11 permafrost coverage over Lena Basin in Siberia. *J. Geophys. Res.*, 114, D07102,
12 doi:10.1029/2008JD010537, 2009.
- 13 Yi, S., Manies, K. L., Harden, J., and McGuire, A. D.: The characteristics of organic soil in
14 black spruce forests: Implications for the application of land surface and ecosystem
15 models in cold regions, *Geophys. Res. Lett.*, 36, L05501, doi:10.1029/2008GL037014,
16 2009a.
- 17 Yi, S., McGuire, A. D., Harden, J., Kasischke, E., Manies, K. L., Hinzman, L. D., Liljedahl,
18 A., Randerson, J. T., Liu, H., Romanovsky, V. E., Marchenko, S., and Kim, Y.:
19 Interactions between soil thermal and hydrological dynamics in the response of Alaska
20 ecosystems to fire disturbance , *J. Geophys. Res.*, 114, G02015,
21 doi:10.1029/2008JG000841, 2009b.
- 22 Yi, S., McGuire, A. D., Kasischke, E., Harden, J., Manies, K. L., Mack, M., and Turetsky, M.
23 R.: A Dynamic organic soil biogeochemical model for simulating the effects of wildfire
24 on soil environmental conditions and carbon dynamics of black spruce forests, *J.*
25 *Geophys. Res.*, 115, G04015, doi:10.1029/2010JG001302, 2010.
- 26 Yi. S., Li, N., Xiang, B., Ye, B. and McGuire, A.D.: Representing the effects of alpine
27 grassland vegetation cover on the simulation of soil thermal dynamics by ecosystem
28 models applied to the Qinghai-Tibetan Plateau, *J. Geophys. Res.*, 118, 1-14, doi:
29 10.1002/jgrg.20093, 2013.
- 30 Yi, S., Wang, X., Qin, Y., Xiang, B., and Ding, Y.: Responses of alpine grassland on
31 Qinghai-Tibetan plateau to climate warming and permafrost degradation: a modeling
32 perspective. *Environ. Res. Lett.*, 9, 074014, doi:10.1088/1748-9326/9/7/074014, 2014a.

- 1 Yi, S., Wischnewski, K., Langer, M., Muster, S., Boike, J.: Modeling different freeze/thaw
2 processes in heterogeneous landscapes of the Arctic polygonal tundra using an ecosystem
3 model. *Geoscientific Model Development*, 7, 1671–1689, 2014b.
- 4 Yi S, FragMAP: a tool for long-term and cooperative monitoring and analysis of small-scale
5 habitat fragmentation using an unmanned aerial vehicle, *International Journal of Remote*
6 *Sensing*, 38:2686-2697, 2017.
- 7 Yin, G., Niu, F., Lin, Z., Luo, J., and Liu, M.: Effects of local factors and climate on
8 permafrost conditions and distribution in Beiluhe basin, Qinghai-Tibet Plateau, China.
9 *Science of the Total Environment*, 581-582, 472-485, 2017.
- 10 Yuan, F. M., Yi, S. H., McGuire, A. D., Johnson, K. D., Liang, J., Harden, J. W., ... and Kurz,
11 W. A.: Assessment of boreal forest historical C dynamics in the Yukon River Basin:
12 relative roles of warming and fire regime change *Ecol. Appl.*, 22, 2091-2109, 2012.
- 13 Zhang, Z. F., and Ward, A. L.: Determining the porosity and saturated hydraulic conductivity
14 of binary mixtures, *Vadose Zone J.*, 10, 313-321, 2011.
- 15 Zhuang, Q., V. E. Romanovsky, and A. D. McGuire: Incorporation of a permafrost model into
16 a large-scale ecosystem model: Evaluation of temporal and spatial scaling issues in
17 simulating soil thermal dynamics, *J. Geophys. Res.*, 106(D24), 33649-33670, 2001.
- 18 Zhuang, Q., J. Melillo, D. Kicklighter, R. G. Prinn, A. D. McGuire, P. A. Steudler, B. S.
19 Felzer, and S. Hu: Methane fluxes between terrestrial ecosystems and the atmosphere at
20 northern high latitudes during the past century: A retrospective analysis with a process-
21 based biogeochemistry model, *Global Biogeochem. Cy.*, 18, GB3010,
22 doi:10.1029/2004GB002239, 2004.
- 23 Zhuang, Q., J. He, Y. Lu, L. Ji, J. Xiao, and T. Luo: Carbon dynamics of terrestrial
24 ecosystems on the Tibetan Plateau during the 20th century: an analysis with a process-
25 based biogeochemical model, *Global Ecol. Biogeogr.*, 19, 649-662, 2010.
- 26 Zou, D., L. Zhao, Y. Sheng, J. Chen, G. Hu, T. Wu, J. Wu, C. Xie, X. Wu, Q. Pang, W. Wang,
27 E. Du, W. Li, G. Liu, J. Li, Y. Qin, Y. Qiao, Z. Wang, J. Shi, and G. Cheng: A new map
28 of permafrost distribution on the Tibetan Plateau, *The Cryosphere*, 11, 2527-2542, 2017.
- 29

1 **Table 1.** The mean (standard deviation in brackets) of measured soil bulk density, calculated
2 porosity from bulk density, measured porosity of different layers based on soil samples in this
3 study.

4

Layer (cm)	Bulk density (g cm ⁻³)	Calculated Porosity (%)	Measured porosity (%)
0—10	1.74 (0.21)	34.4 (0.08)	28.4 (0.03)
10—20	1.81 (0.11)	31.8 (0.04)	27.7 (0.02)
20—30	1.86 (0.32)	29.7 (0.12)	30.2 (0.05)
40—50	1.61 (0.23)	39.4 (0.09)	29.6 (0.02)
70—80	1.62 (0.20)	38.8 (0.08)	20.6 (0.11)
110—120	1.75 (0.09)	33.9 (0.04)	27.7 (0.01)
150—160	1.70 (0.15)	36.0 (0.06)	26.3 (0.02)
190—200	1.81 (0.09)	31.6 (0.03)	27.1 (0.02)

5

1 **Table 2.** The particle size diameter fractions (for >2 mm this is the mass ratio between soil
2 particles greater than 2 mm and total soil sample, while for the other fractions this is the ratio
3 between mass of the soil in the size range and the mass of all particles < 2mm) and soil
4 texture (based on USDA classification) of different layers based on soil samples in this study.
5

Layer (cm)	>2 mm	>63 μ m	2-63 μ m	<2 μ m	Texture
0—10	0.38 (0.07)	0.77 (0.07)	0.18 (0.04)	0.05 (0.02)	Loamy sand
10—20	0.52 (0.14)	0.72 (0.11)	0.20 (0.05)	0.07 (0.05)	Loamy sand
20—30	0.55 (0.17)	0.69 (0.09)	0.24 (0.08)	0.07 (0.01)	Sandy loam
40—50	0.55 (0.19)	0.70 (0.13)	0.26 (0.11)	0.04 (0.02)	Loamy sand
70—80	0.65 (0.16)	0.71 (0.09)	0.25 (0.07)	0.04 (0.02)	Loamy sand
110—120	0.63 (0.05)	0.79 (0.09)	0.19 (0.08)	0.03 (0.02)	Loamy sand
150—160	0.63 (0.09)	0.85 (0.04)	0.13 (0.03)	0.02 (0.01)	Loamy sand
190—200	0.50 (0.19)	0.71 (0.19)	0.24 (0.14)	0.05 (0.05)	Loamy sand

6
7
8

1 **Table 3.** The mean (standard deviation in brackets) of the measured frozen and unfrozen dry
 2 and saturated soil thermal conductivity ($W\ m^{-1}\ K^{-1}$) of different soil layers.

3

Layer (cm)	Dry		Saturated	
	Unfrozen	Frozen	Unfrozen	Frozen
0-10	0.238 (0.09)	0.414 (0.09)	2.322 (0.17)	3.122 (0.48)
10~20	0.340 (0.04)	0.365 (0.23)	2.147 (0.47)	3.193 (0.55)
20-30	0.395 (0.07)	0.420 (0.11)	2.743 (0.38)	3.059 (0.29)
40-50	0.346 (0.00)	0.388 (0.14)	2.539 (0.30)	3.184 (0.33)
70-80	0.340 (0.03)	0.289 (0.12)	2.589 (0.16)	3.362 (0.38)
110-120	0.400 (0.06)	0.271 (0.07)	2.616 (0.11)	3.721 (0.05)
150-160	0.401 (0.01)	0.248 (0.07)	2.246 (0.19)	3.647 (0.48)
190-200	0.399 (0.26)	0.392 (0.14)	2.609 (0.12)	3.329 (0.19)

4

5

1 **Table 4.** The mean (standard deviation) of measured saturated hydraulic conductivity (K_{sat} ;
 2 mm s⁻¹) and fitted absolute value of saturated matric potential (Ψ_{sat} ; mm), fitted pore size
 3 distribution parameter (B) and the correlation coefficients (R^2) between calculated matric
 4 potential using fitted equations and measured.

5

Layer (cm)	K_{sat}	Matric potential		
		Ψ_{sat}	B	R^2
0-10	0.0285 (0.0274)	49.14	4.03	0.991
10~20	0.0056 (0.0036)	70.66	4.49	0.996
20-30	0.0047 (0.0027)	27.02	5.22	0.994
40-50	0.0078 (0.0043)	143.4	3.59	0.994
70-80	0.0072 (0.0054)	179.6	3.22	0.993
110-120	0.0315 (0.0054)	603.7	1.89	0.969
150-160	0.0053 (0.0028)	49.17	2.97	0.993
190-200	0.0036 (0.0023)	14.47	4.565	0.989

6

7

1 **Table 5.** Model performance when default sand parameters are substituted with combinations
 2 of measured porosity (I), thermal conductivity (II), hydraulic conductivity (III) and matric
 3 potential (IV).

	Best	I	II	III	IV	V	VI	VII	VIII	IX	X	All
	II	III	V	III	IV	III	II	II	III	III		
						V	III	IV	IV	IV		
100 cm ST	II											
ALD	I	1										
PLB	II	1	2									
10 cm SM	I	7	2	4			1	5	6			3
40 cm SM	I											
80 cm SM	I	7	1	4			2	6	5			3
160 cm CM	I	1										

4 **Note:** Best column shows the model simulations (individual parameter substitution) with the
 5 smallest root mean squared error (RMSE) for 100 cm soil temperature (ST, °C), active layer
 6 depth (ALD, m), permafrost low boundary (PLB, m), 10, 40, 80 and 160 cm soil liquid water
 7 content (SM, -); Numbers indicate the combination of parameters that have smaller RMSE
 8 than the best model run using individual parameter substitution. “All” indicates the
 9 combination of all 4 parameters. The smallest number indicates the smallest RMSE.

10
 11
 12
 13

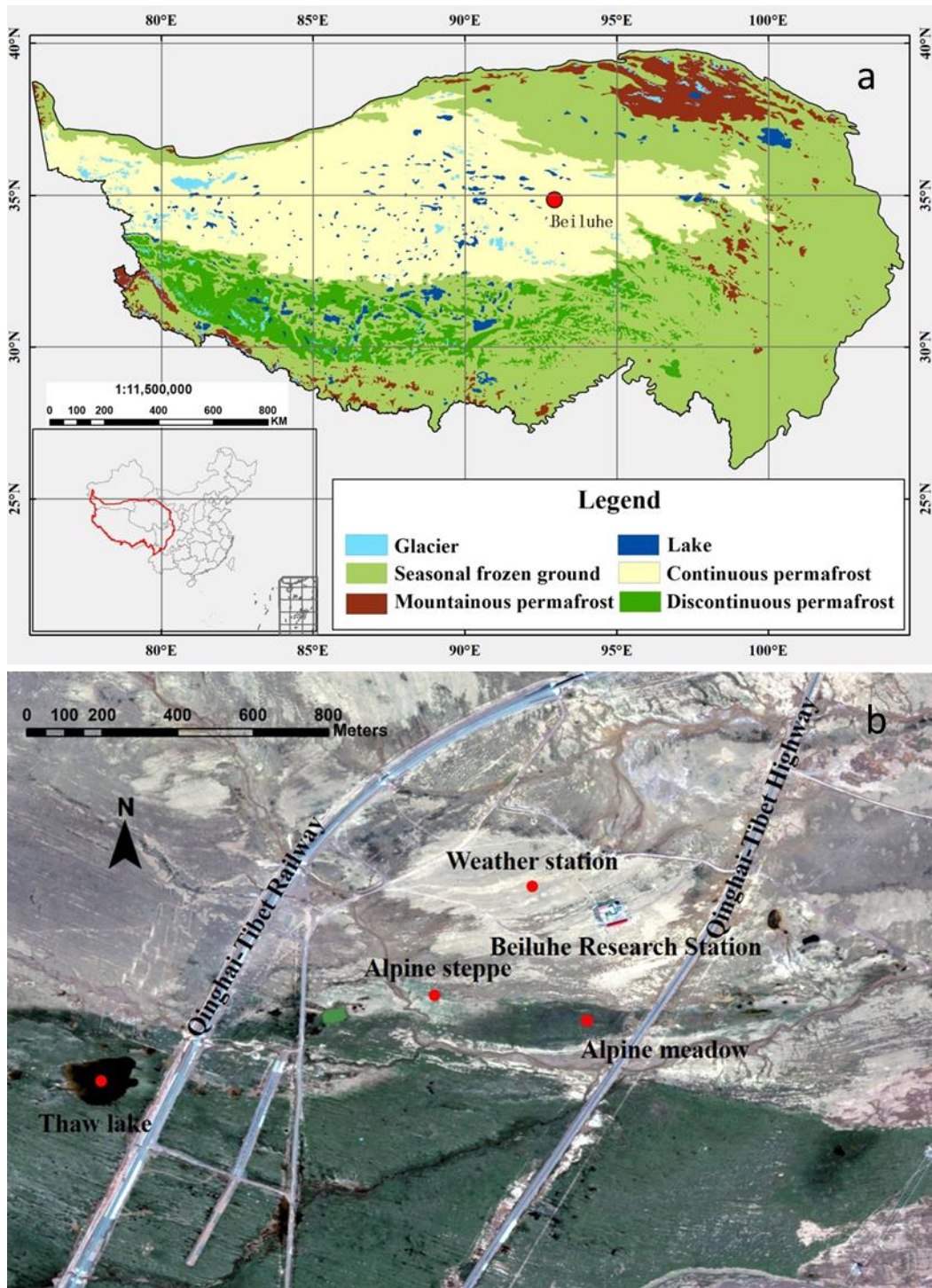
1 **Table 6** Model performance when default loam parameters are substituted with combinations
 2 of measured porosity (I), thermal conductivity (II), hydraulic conductivity (III) and matric
 3 potential (IV) .

4

	Best	I	I	I	II	II	I	I	I	I	II	All
		II	III	IV	III	IV	III	II	II	III	III	
							V	III	IV	IV	IV	
100 cm ST	I	1		2					3			
ALD	I	3	5					1	2	6		4
PLB	II											
10 cm SM	I	7	6	1				5	2	4		3
40 cm SM	I	5	7	1				6	3	4		2
80 cm SM	I											
160 cm SM	I	1	3					2				

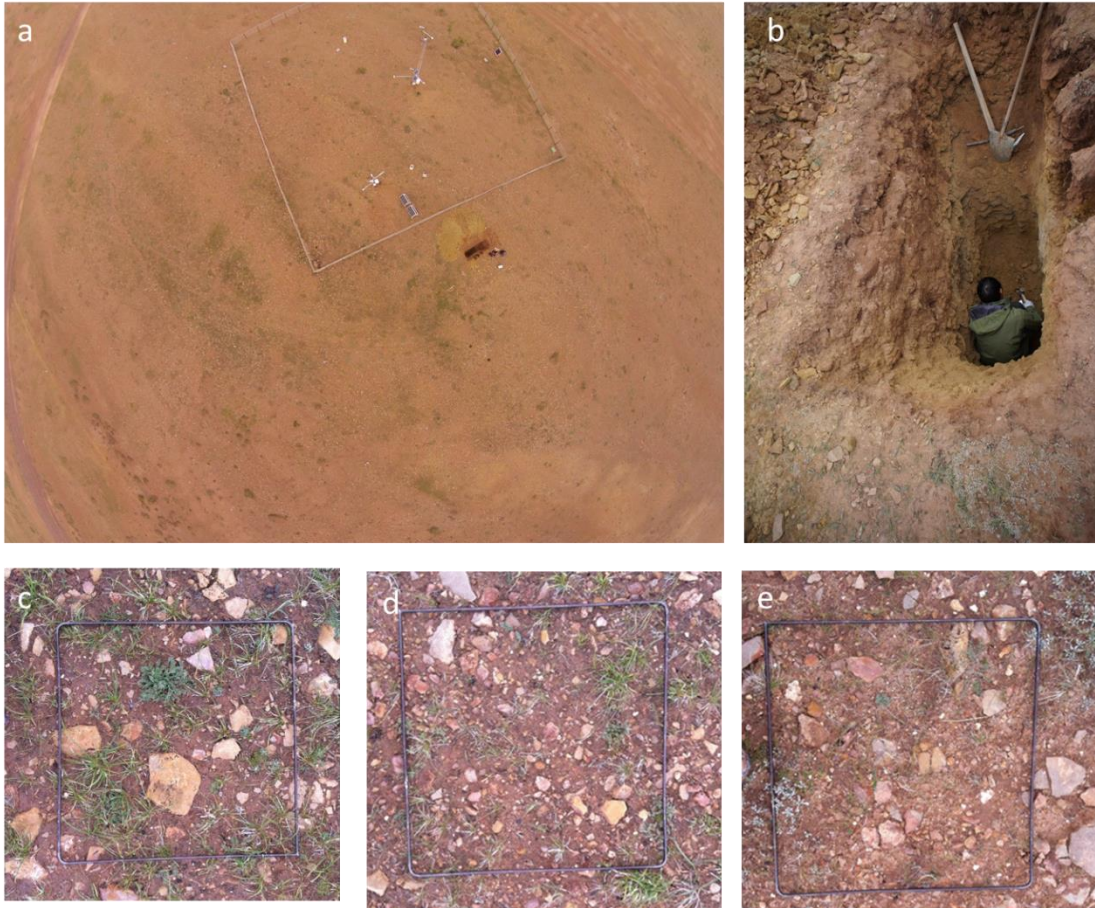
5
 6 **Note:** Best column shows the model simulations (individual parameter substitution) with the
 7 smallest root mean squared error (RMSE) for 100 cm soil temperature (ST, °C), active layer
 8 depth (ALD, m), permafrost low boundary (PLB, m), 10, 40, 80 and 160 cm soil liquid water
 9 content (SM, -); Numbers indicate the combination of parameters that have smaller RMSE
 10 than the best model run using individual parameter substitution. “All” indicates the
 11 combination of all 4 parameters. The smallest number indicates the smallest RMSE.

1 **Figure 1. a)** Locations of a) Beiluhe permafrost station on the Qinghai-Tibetan Plateau, and b)
2 the googlemap of the weather station and the surrounding environment.



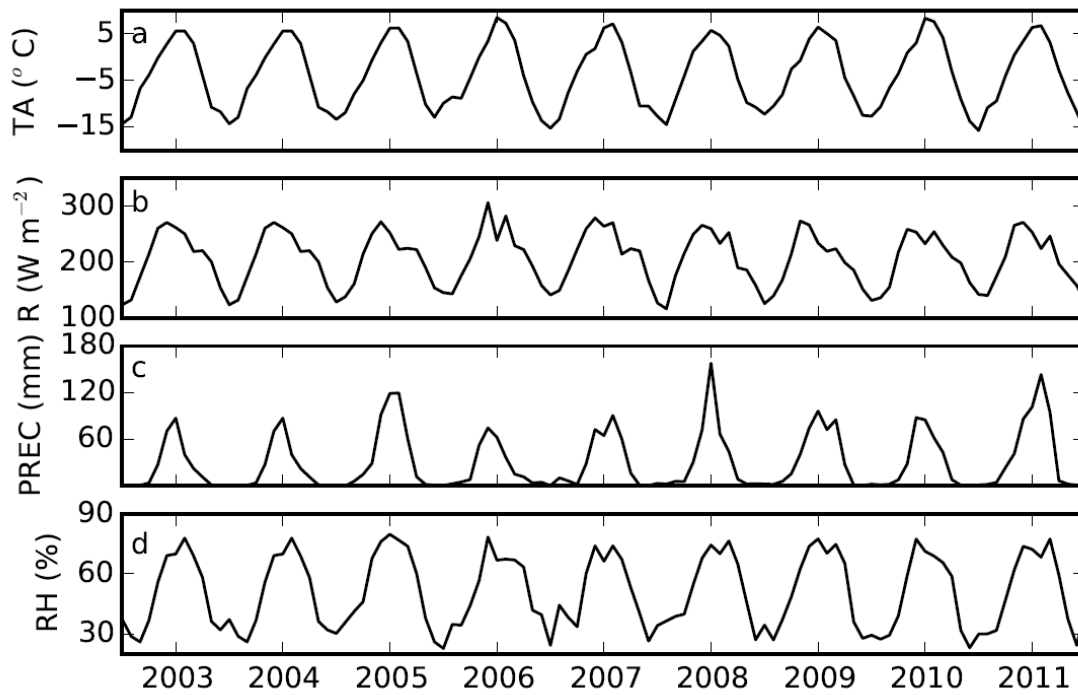
3
4

1 **Figure 2.** Images of site conditions: **a)** the aerial view of the weather station and the
2 excavated soil pit (the borehole is located in the lower left corner of white fence); **b)** the
3 detailed view of the excavated soil pit; and **c)-e)** examples of vegetation, gravel and stones
4 (iron frame is about 0.5 m×0.5 m).



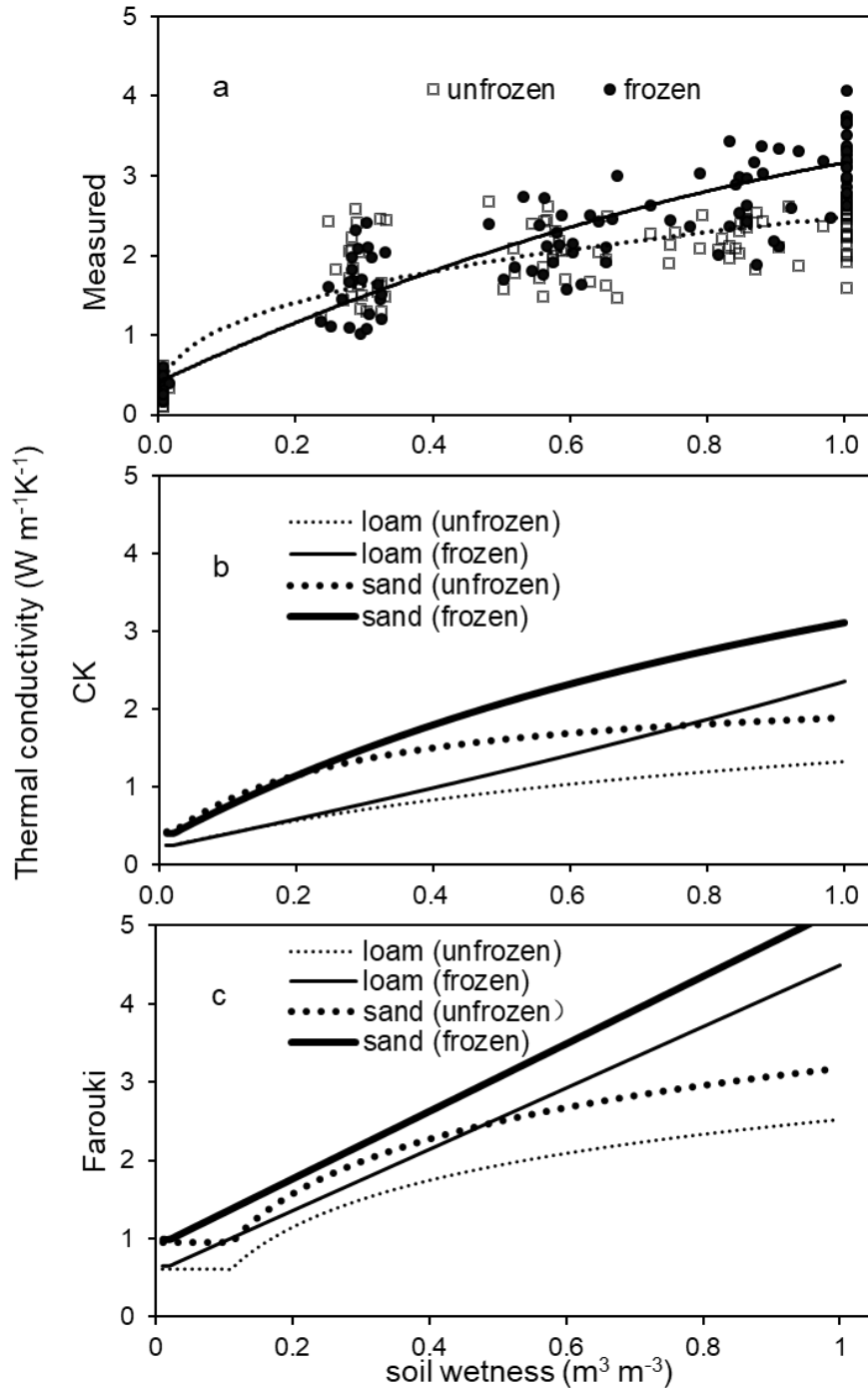
5
6
7
8

- 1 **Figure 3.** Time series of data measured at the Beiluhe weather station, Qinghai-Tibetan
- 2 Plateau, 2003 to 2011: **a)** air temperature (TA, °C); **b)** downward solar radiation (R, W m⁻²); **c)**
- 3 precipitation (PREC, mm) and **d)** relative humidity (RH, %).



4

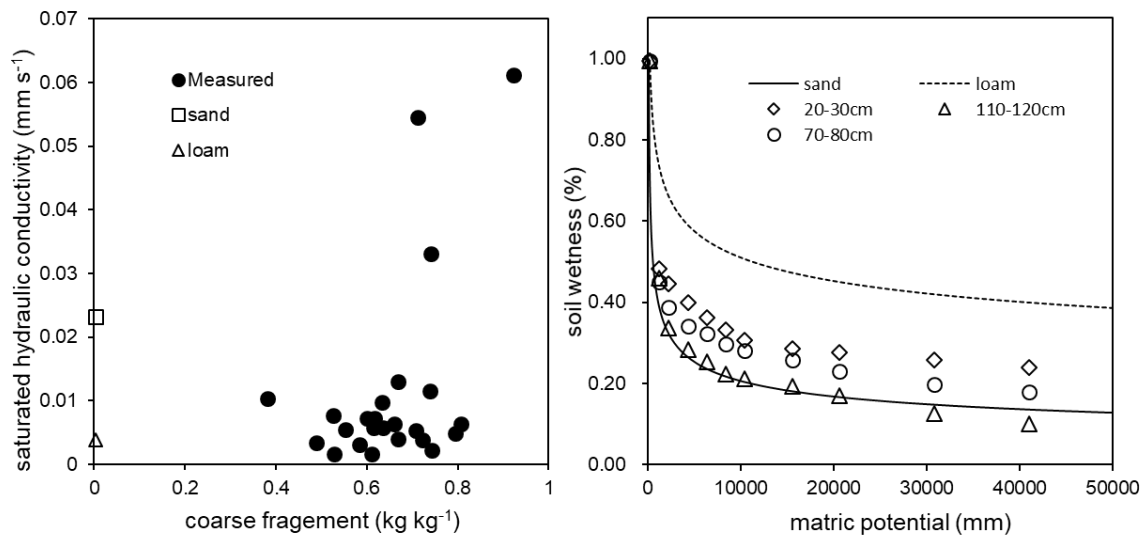
1 **Figure 4.** The relationship between soil wetness (solid and dotted lines represent frozen and
 2 unfrozen cases) and soil thermal conductivity ($\text{W m}^{-1}\text{K}^{-1}$) from: **a)** measured values
 3 (Measured; dots and empty diamonds represent measured frozen and unfrozen soil thermal
 4 conductivities, respectively), **b)** using the Côté and Konrad (2005) scheme (CK); and **c)** using
 5 the Farouki (1986) scheme (Farouki). Thick and thin lines represent relationships for sand and
 6 loam, respectively.



7
8

1 **Figure 5.**The relations between **a**) saturated hydraulic conductivity (mm s^{-1}) and coarse
 2 fragment fraction (Solid dots represent measured value; empty circle and empty triangle
 3 represent the corresponding values of sand and loam used in Community Land Model,
 4 respectively), and **b**) soil wetness (lines) and absolute value of matric potential ($\text{mm H}_2\text{O}$) at
 5 three representative depths (solid and dashed lines represent default values (Oleson et al.,
 6 2010) of sand and loam, respectively).

7

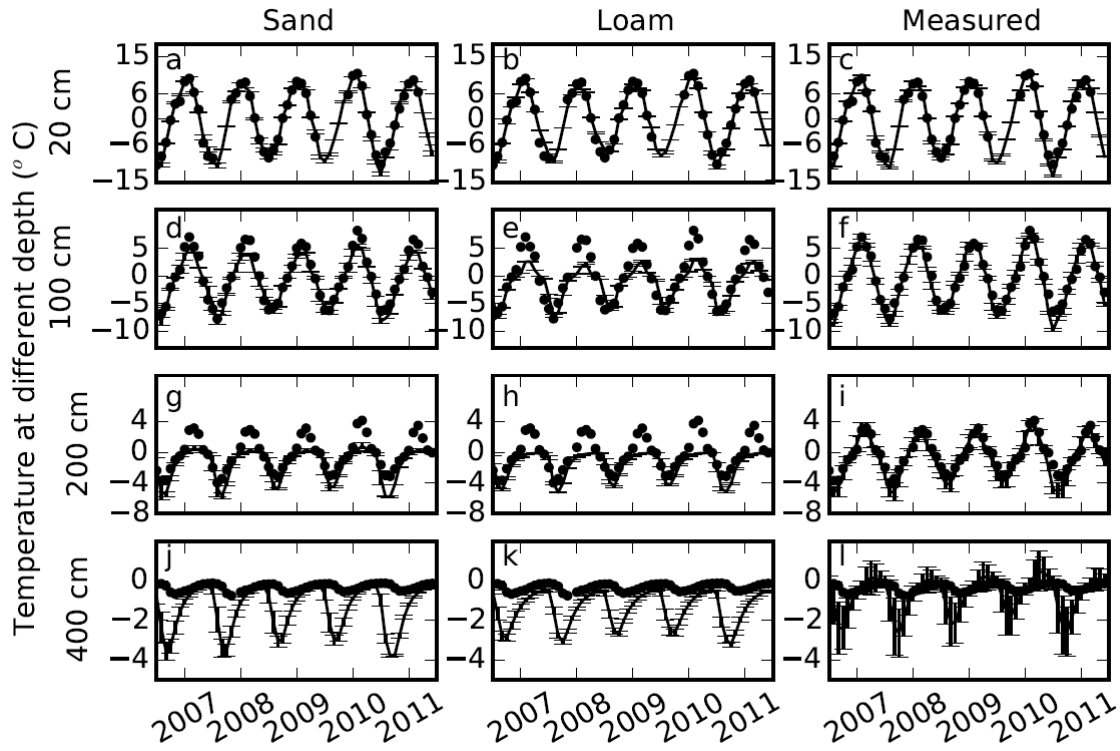


8

9

1 **Figure 6.** Comparisons of soil temperatures simulated using default parameters for sand, loam,
2 and our measured parameters (lines) with measured soil temperatures (dots) at 20, 100, 200
3 and 400 cm depths. Error bars show the standard deviations calculated based on 9 simulations
4 with 3 different slopes and 3 different soil thicknesses.

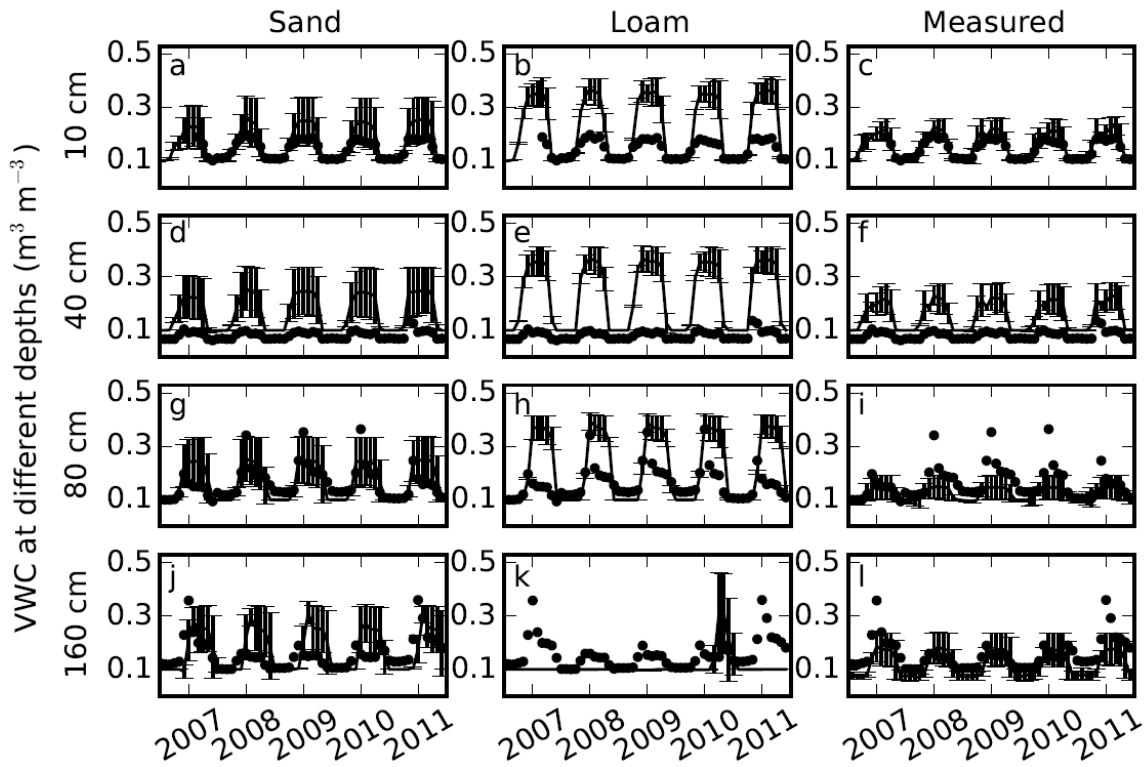
5



6

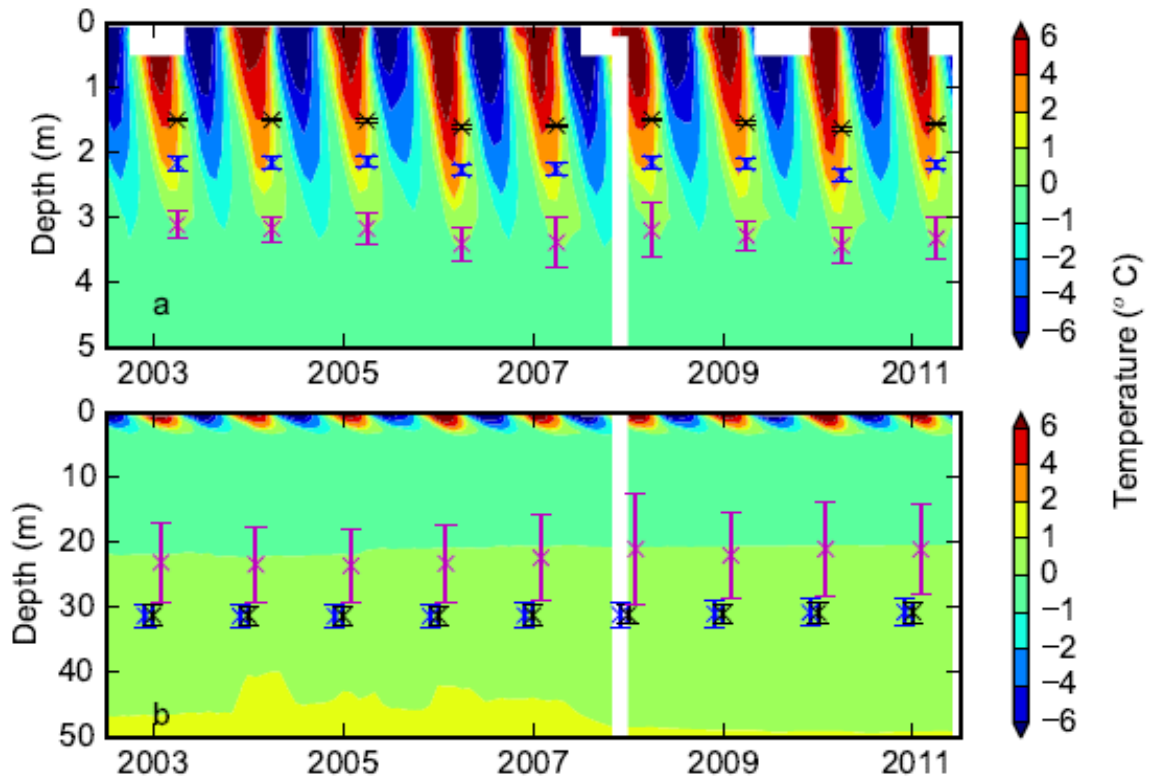
7

1 **Figure 7.** Comparisons of soil volumetric liquid water content (VWC) simulated using
 2 default parameters sand, default loam, and measured parameters (lines) with measured soil
 3 moistures (dots) at 10, 40, 80 and 160 cm depths. Error bars showed the standard deviation
 4 calculated based on 9 simulations with 3 different slopes and 3 different soil thicknesses.



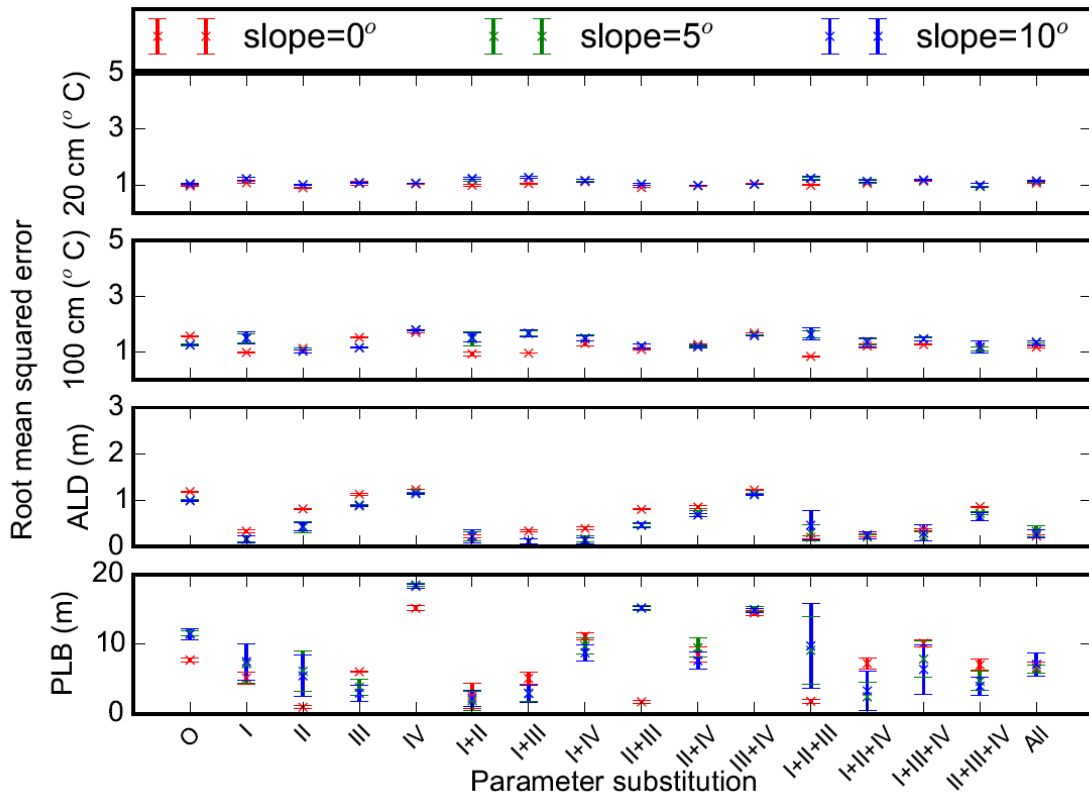
5
 6
 7

1 **Figure 8.** Contour plots showing **a)** soil temperature ($^{\circ}\text{C}$) from borehole measurements down
2 to 5 m superimposed with simulated active layer depths over the period of 2003-2011; and **b)**
3 ground temperature down to 50 m superimposed with the simulated permafrost low boundary.
4 Black, blue and magenta represent simulations with loam, sand and measured parameters,
5 respectively. Error bars show the standard deviation calculated based on 9 simulations with 3
6 different slopes and 3 different soil thicknesses.



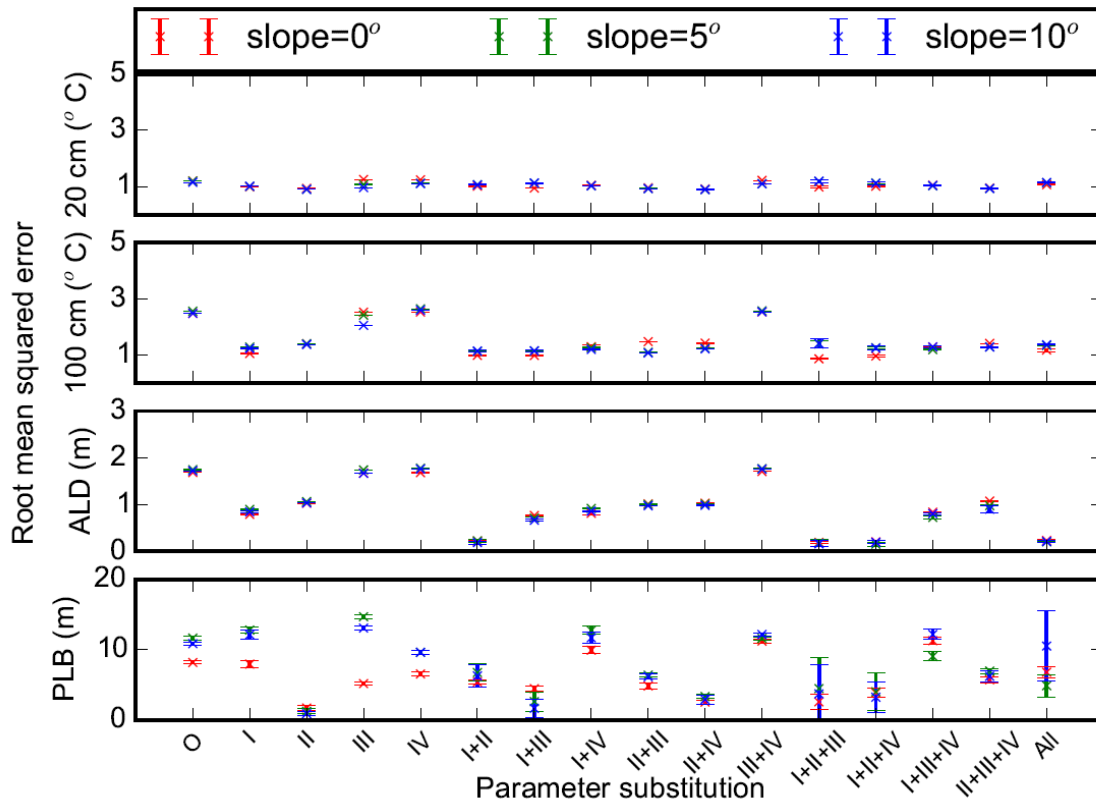
7
8
9
10
11

1 **Figure 9.** Root mean squared errors between measurements and model simulations (with
 2 different combinations of measured porosity (I), thermal conductivity (II), hydraulic
 3 conductivity (III) and matric potential (IV) of default sand parameters) for 20 and 100 cm soil
 4 temperatures ($^{\circ}\text{C}$), active layer depth (ALD, m) and permafrost low boundary (PLB, m). O
 5 and All represent model runs without substitution of default parameters and with all 4
 6 parameters substituted, respectively. Mean and standard deviation of model simulations with
 7 3 different soil thicknesses at each slope (0° , 5° , and 10°) are shown.



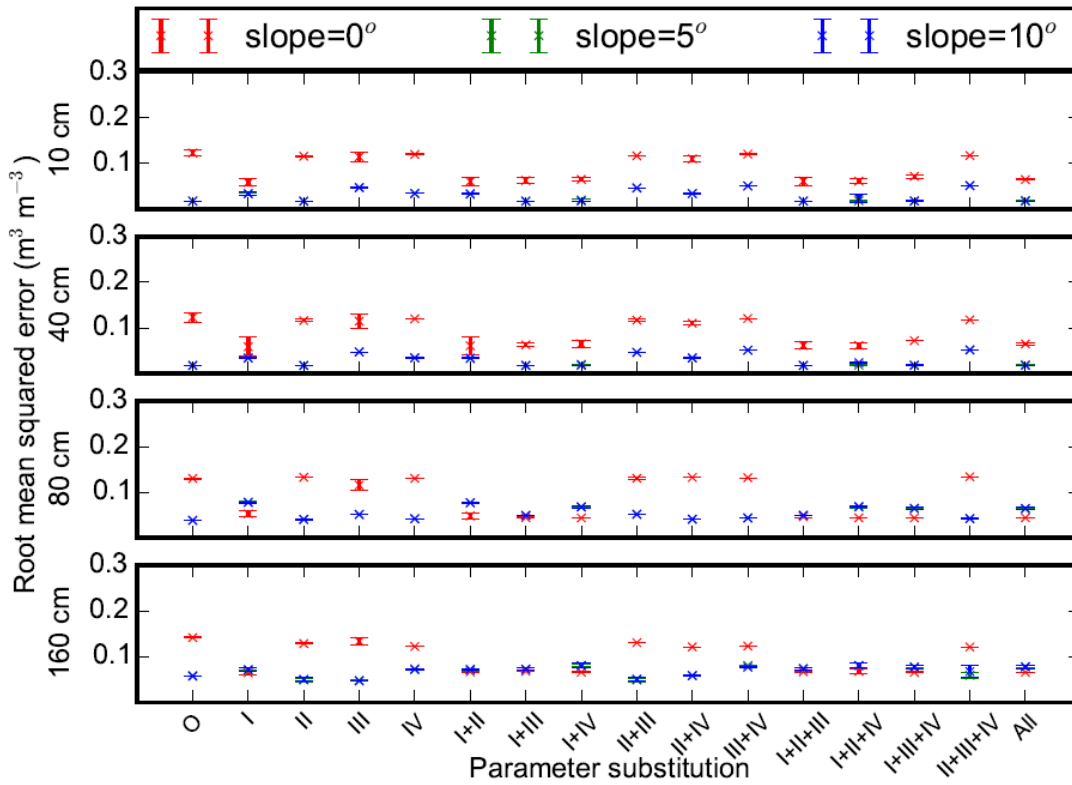
8
 9
 10

1 **Figure 10.** Root mean squared errors between measurements and model simulations (with
 2 different combinations of measured porosity (I), thermal conductivity (II), hydraulic
 3 conductivity (III) and matric potential (IV) of default loam parameters) for 20 and 100 cm soil
 4 temperatures ($^{\circ}\text{C}$), active layer depth (ALD, m) and permafrost low boundary (PLB, m). O
 5 and All represent model runs without substitution of default parameters and with all 4
 6 parameters substituted, respectively. Mean and standard deviation of model simulations with
 7 3 different soil thicknesses at each slope (0° , 5° , and 10°) are shown.



8
 9
 10
 11
 12
 13

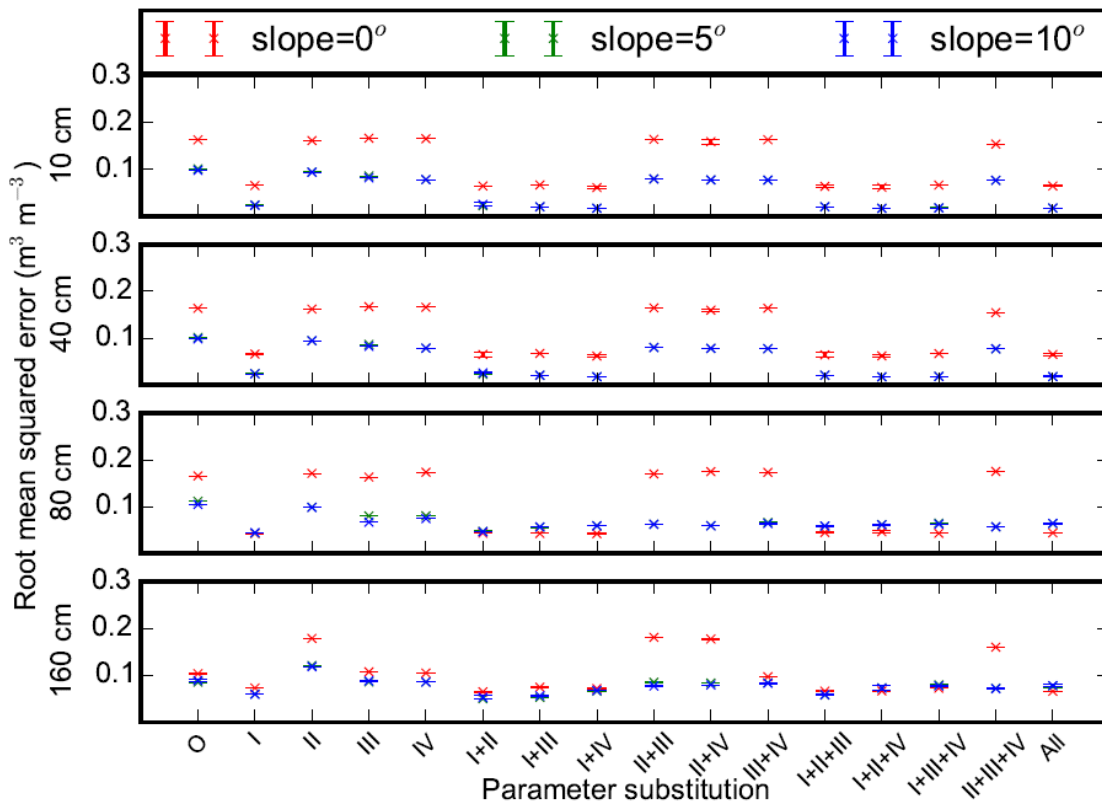
1 **Figure 11.** Root mean squared errors between measurements and model simulations (with
 2 different combinations of measured porosity (I), thermal conductivity (II), hydraulic
 3 conductivity (III) and matric potential (IV) of default sand parameters) for 10 cm, 40 cm, 80
 4 cm and 160 cm soil volumetric liquid water content. O and All represent model runs without
 5 substitution of default parameters and with all 4 parameters substituted, respectively. Mean
 6 and standard deviation of model simulations with 3 different soil thicknesses at each slope (0° ,
 7 5° , and 10°) are shown.



8
 9
 10

1 **Figure 12.** Root mean squared errors between measurements and model simulations (with
 2 different combinations of measured porosity (I), thermal conductivity (II), hydraulic
 3 conductivity (III) and matric potential (IV) of default loam parameters) for 10 cm, 40 cm, 80
 4 cm and 160 cm soil volumetric liquid water content. O and All represent model runs without
 5 substitution of default parameters and with all 4 parameters substituted, respectively. Mean
 6 and standard deviation of model simulations with 3 different soil thicknesses at each slope (0° ,
 7 5° , and 10°) are shown.

8



9

10